

# Interaction of eta mesons with nuclei

N G Kelkar<sup>1,†</sup>, K P Khemchandani<sup>2,††</sup>, N J Upadhyay<sup>3,\*</sup> and B K Jain<sup>4,\*\*</sup>

<sup>1</sup> Dept. de Física, Univ. de los Andes, Cra 1E, 18A-10, Bogota, Colombia

<sup>2</sup> Instituto de Física, Universidade de São Paulo, C.P. 66318, 05389-970 São Paulo, SP, Brazil

<sup>3</sup> National Superconducting Cyclotron Laboratory, Michigan State University, East Lansing, Michigan 48824-1321, USA

<sup>4</sup> MU-DAE Centre for Excellence in Basic Sciences, Mumbai University, Mumbai 400098, India

E-mail: <sup>†</sup>nkelkar@uniandes.edu.co, <sup>††</sup>kanchan@if.usp.br, <sup>\*</sup>upadhyay@nscl.msu.edu, <sup>\*\*</sup>brajeshk@gmail.com

**Abstract.** Back in the mid eighties, a new branch of investigation which was related to the interaction of eta mesons with nuclei came into existence. It started with the theoretical prediction of possible exotic states of eta mesons and nuclei bound by the strong interaction and later developed into an extensive experimental program to search for such unstable states as well as understand the underlying interaction via eta meson producing reactions. The vast literature of experimental as well as theoretical works which studied various aspects of eta producing reactions such as the  $\pi^+ n \rightarrow \eta p$ ,  $pd \rightarrow {}^3\text{He } \eta$ ,  $p {}^6\text{Li} \rightarrow {}^7\text{Be } \eta$  and  $\gamma {}^3\text{He} \rightarrow \eta X$ , to name a few, had but one objective in mind: to understand the eta - nucleon ( $\eta N$ ) and hence the  $\eta$ -nucleus interaction which could explain the production data and confirm the existence of some  $\eta$ -mesic nuclei. In spite of these efforts, there remain uncertainties in the knowledge of the  $\eta N$  and hence the  $\eta$ -nucleus interaction. The present work is hence an attempt to bind together the findings in these works and draw some global and specific conclusions which can be useful for future explorations.

The  $\eta N$  scattering length (which represents the strength of the  $\eta$  - nucleon interaction) using different theoretical models and analysing the data on  $\eta$  production in pion, photon and proton induced reactions was found to be spread out in a wide range, namely,  $0.18 \leq \Re a_{\eta N} \leq 1.03$  fm and  $0.16 \leq \Im a_{\eta N} \leq 0.49$  fm. Theoretical searches of heavy  $\eta$ -mesic nuclei based on  $\eta$ -nucleus optical potentials and lighter ones based on Faddeev type few body approaches predict the existence of several quasibound and resonant states. Though some hints of  $\eta$ -mesic states such as  ${}^3_\eta\text{He}$  and  ${}^{25}_\eta\text{Mg}$  do exist from previous experiments, the promise of clearer signals for the existence of  $\eta$ -mesic nuclei lies in the experiments to be performed at the J-PARC, MAMI and COSY facilities in the near future. This review is aimed at giving an overall status of these efforts.

PACS numbers: 25.10.+s, 21.85.+d, 13.75.-n, 13.60.Le

## Contents

<b>1</b>	<b>Introduction</b>	<b>2</b>
<b>2</b>	<b><math>\eta</math>-nucleon interaction and scattering amplitude</b>	<b>7</b>
2.1	Phenomenological . . . . .	8
2.2	Theoretical . . . . .	10
<b>3</b>	<b>Searches for unstable eta-mesic nuclei</b>	<b>11</b>
3.1	Experimental searches . . . . .	11
3.1.1	Eta meson production in proton induced reactions . . . . .	12
3.1.2	Photoproduction and quasibound states . . . . .	16
3.1.3	Eta production with pion beams . . . . .	17
3.2	Theoretical studies . . . . .	17
3.2.1	Few body equations and unstable states of light nuclei . . . . .	18
3.2.2	Optical potential approaches for heavy $\eta$ -mesic nuclei . . . . .	20
3.2.3	Collision times of eta mesons and light nuclei . . . . .	22
<b>4</b>	<b>Reaction mechanisms for meson production</b>	<b>26</b>
4.1	One, two and three body mechanisms . . . . .	26
4.2	Proton induced $\eta$ production on light nuclei and cross section features near threshold . . . . .	27
4.3	Meson exchange model for eta production at high energies . . . . .	30
4.3.1	$pp \rightarrow pp\eta$ reaction . . . . .	31
4.3.2	$pd \rightarrow {}^3\text{He} \eta$ . . . . .	32
<b>5</b>	<b>Eta meson interaction with nuclei in the final state</b>	<b>34</b>
5.1	Approximate methods and the need for few body equations . . . . .	34
5.1.1	Scattering length approximation . . . . .	34
5.1.2	Half-off-shell $\eta$ -nucleus T-matrix . . . . .	35
5.2	Final state $\eta$ nucleus interaction in proton induced reactions . . . . .	36
5.2.1	The $pn \rightarrow d\eta$ reaction . . . . .	37
5.2.2	The $pd \rightarrow pd\eta$ reaction . . . . .	38
5.2.3	Cluster model approach to the $p{}^6\text{Li} \rightarrow \eta {}^7\text{Be}$ reaction . . . . .	41
<b>6</b>	<b>Summary</b>	<b>43</b>

## 1. Introduction

Meson related physics has always led to interesting findings in different ways. Though mesons are strongly interacting objects composed of quark - antiquark ( $q\bar{q}$ ) pairs, the

bonding of electrically charged mesons with nuclei leads to the formation of exotic atoms. For example, negatively charged pions or kaons could replace an electron in an outer orbital in a standard atom and get bound in the atom due to the Coulomb interaction. After some transitions to lower states however, the meson comes within the range of the strong nuclear interaction and is absorbed on to the nucleus or lost in a nuclear reaction. Thus a meson which in principle in free space could have undergone a weak decay gets bound by the electromagnetic interaction and vanishes by the strong interaction. There exists yet another possibility for the formation of bound states of mesons and nuclei and this is when the meson-nucleus strong interaction is attractive (which may not necessarily be the case). The eta ( $\eta$ ) meson seems to satisfy this requirement. Its interaction with the nucleon in the s-wave (which proceeds through the formation of an  $N^*(1535)$  nucleon resonance) was found to be attractive [1] and led to the prediction [2, 3, 4] and early searches [5] of unstable states of eta mesons and nuclei. The existence of unstable bound states of the strange  $K$ -meson and nuclei was also indicated in some recent experiments as a result of the  $K^-p$  s-wave interaction [6, 7]. Additionally, the superposition of a large repulsive s-wave  $\pi^-$ -nucleus interaction at low pion momenta and an attractive Coulomb interaction has been seen to give rise to deeply bound pion-nucleus bound states [8].

The interaction of the  $\eta$ -meson with a nucleon near threshold is mainly determined by the  $S_{11}$ ,  $J^\pi(\text{spin}^{\text{parity}}) = \frac{1}{2}^-$  resonance  $N^*(1535)$ , which is just 49 MeV above the  $\eta N$  threshold and has a width  $\Gamma=150$  MeV, thus covering the whole low energy region of the  $\eta N$  interaction. As the  $S_{11}$ -resonance also decays to  $\pi N$ ,  $\gamma N$  and  $\pi\pi N$  channels, the correct treatment of the  $\eta N$  interaction, therefore, involves its coupling to all these channels. Several such coupled channel calculations have been reported in literature [9, 10, 11, 12, 13, 14, 15]. Results of these calculations are fitted to the available data, and the  $\eta N$  scattering amplitude is obtained. However, as the fitted data do not include the elastic  $\eta N$  scattering data due to nonavailability of  $\eta$  beams, such extracted  $\eta N$  scattering amplitudes and hence the  $\eta N$  scattering lengths,  $a_{\eta N}$ , have uncertainties. But one conclusion which seems definite in all the calculations is that the  $\eta N$  interaction is strong and attractive in the s-wave.

When viewed as an elementary particle, the  $\eta$ -meson is quite similar to the  $\pi^0$ -meson, despite the  $\eta$  being about four times heavier than the  $\pi^0$ . Both mesons are pseudoscalar, i.e.,  $J^\pi = 0^-$ , are charge neutral, have almost the same lifetime ( $10^{-18}$  sec) and are the only mesons that have a high probability of pure radiative decay. Structurally though, as they are the quantum states of  $q\bar{q}$ , it is believed that due to the mass difference between the u and d quarks and their electromagnetic interaction, the  $\pi^0$  and  $\eta$  are not pure isotopic spin states. The physically observed  $\pi^0$  and  $\eta$  are, actually, the superposition of the pure isotopic spin  $T=0$  and 1 quantum states. The value of the mixing angle of these two states obtained in [16] from an analysis of the cross sections for the  $pd \rightarrow {}^3\text{H} \pi^+ / {}^3\text{He} \pi^0$  reactions is  $0.006 \pm 0.005$  radians. Ref. [16] also discusses literature where the values vary between 0.01 to 0.034 radians. The  $\eta$ -meson is also known to mix with its heavier partner,  $\eta'$ . The isospin mixing structure of

the  $\pi^0$  and  $\eta$  gets manifested as isospin symmetry breaking (ISB) and charge symmetry breaking (CSB) when these mesons come in contact with nucleons. Though it is believed that most of the ISB and CSB effects observed in hadronic systems have the above origin, significant and directly observable isospin-violating effects may be seen in pion production at energies near the  $\eta$  threshold via  $\eta-\pi^0$  external mixing. Such exploratory studies have been conducted experimentally and theoretically [17, 18, 19].

Coming back to the  $\eta N$  interaction, its strong attractive nature opened up the possibility of the formation of  $\eta$ -nucleus quasibound states. The initial theoretical prediction around 1986 about the possible existence of unstable bound states of eta mesons and nuclei gave rise to experimental programs to hunt for the existence of eta-mesic states as well as eta meson production experiments aimed at studying the eta-nucleus interaction in the final states. The theoretical developments kept pace with the experiments. Over the years more and more sophisticated models to understand the basic eta-nucleon interaction, the few body problem of eta mesons and light nuclei and the many body problem of eta mesons and heavy nuclei kept appearing. After about 25 years of investigations in this field, there has been a lot of progress and some evidence exists for the existence of such states. However, there is still no general agreement and no final word on the strength of the eta-nucleon and eta-nucleus interaction.

Though a detailed account of the various theoretical and experimental efforts will be given in the next sections of the article, at this point we mention a few of these works. For nuclei beyond few-nucleon systems, calculations have mostly been done using an  $\eta$ -nucleus optical potential. In [2, 3, 20], the  $\eta$ -mesic states were found from complex energy solutions of the momentum-space relativistic three-dimensional integral equation using different optical potentials. In this work, the binding energies and widths were found to strongly depend on the sub-threshold  $\eta$ -nucleon interaction. These calculations predicted unstable bound or quasibound states for nuclei with mass number greater than 10. In another approach using optical potentials [21], the self energies of the  $\eta$  meson in the nuclear medium evaluated for  $^{12}\text{C}$ ,  $^{40}\text{Ca}$  and  $^{208}\text{Pb}$  were used to find the widths of quasibound states of  $\eta$  mesons and nuclei. In [22], the energies and widths of several  $\eta$ -mesic nuclei were predicted by once again using self energies of the  $\eta$  in the medium but evaluated using the technique of unitarized chiral perturbation theory. Another approach that has been used is the QCD based quark-meson-coupling approach (QMC), where the  $\eta$ -meson is embedded in the nuclear medium and couples to quarks and mixes with  $\eta'$  [23, 24]. The  $\eta$  self energy obtained from such calculations was used in the local density approximation in the Klein-Gordon equation to obtain the complex energy solutions. This approach, apart from predicting the energies and widths of the quasibound states also showed the important role of  $\eta-\eta'$  mixing in understanding the  $\eta N$  scattering amplitude.

For few-nucleon systems, the existence of  $\eta$  binding is mostly explored by calculating the poles in the scattering amplitude and the corresponding  $\eta$ -nucleus scattering lengths. The existence of quasibound states requires the real parts of the scattering lengths to be large and negative. In [25] the author predicted a quasibound state in the  $\eta NN$ -

$\pi NN$  coupled system and confirmed its existence through the existence of a pole and a remarkable enhancement of the  $\eta d$  elastic cross section. The state was predicted with a mass of 2430 MeV and a width of 10-20 MeV. In [26, 27, 28] using Faddeev equations and a certain choice of potentials for the binary sub-systems in it, the authors found at best the existence of a quasivirtual state only. Other works involve the use of a multiple scattering formalism [29, 30] and calculations done within the finite rank approximation using few body equations [31, 32, 33] to characterize  $\eta$ -mesic states of the deuteron,  ${}^3\text{H}$ ,  ${}^3\text{He}$  and  ${}^4\text{He}$  nuclei. These and other few body calculations will be discussed in detail in section 3.

The anticipated  $\eta$ -nucleus bound states should get reflected in a straight forward way in the measured eta producing nuclear cross sections. Such observations have indeed been made in the proton induced  $\eta$  production reactions where the measured amplitude on the deuteron target shows a sharp rise as one approaches the threshold [34, 35, 36, 37, 38] of  $\eta$  production. The  $\eta$   ${}^3\text{He}$  (or  $\eta d$ ) scattering amplitude has been usually extracted from data by writing the cross section as a product of the plane wave result and an enhancement factor, which has been parametrized in terms of the scattering length [39]. Large values of the real part of the extracted scattering lengths from such analyses are normally taken as an indicator for the existence of bound states. This procedure of extracting the scattering lengths, however, ignores reference to any reaction mechanism for  $\eta$  production and lacks a detailed treatment of the final state interaction. Therefore, while the extracted scattering lengths by this method may at best be indicative, their actual values may not be fully reliable for determining the bound states. A proper procedure should be to first analyze these data using a certain  $\eta$  production mechanism [40] and then incorporate in detail the final state interaction (FSI) as accurately as possible. Once such a procedure, using the available  $\eta N$  transition matrix, reproduces the measured cross sections, one can then infer from them the resultant  $\eta$ -nucleus scattering amplitudes, which will have a certain in-built off-shell behaviour. These amplitudes can then be used to investigate the possibility of the existence of unstable bound states. Based on this concept the present authors first carried out a systematic analysis of the  $\eta$  producing nuclear reactions to obtain a reliable  $\eta$ -nucleus scattering amplitude which was then used to locate the unstable bound states in the  $\eta$ -deuteron,  $\eta$ - ${}^3\text{He}$  and  $\eta$ - ${}^4\text{He}$  systems [41]. The states were located using Wigner's time delay method which had earlier been successfully used to locate meson and baryon resonances [42, 43]. A modification of Wigner's method was done in [44] and an eta-mesic state in the  $\eta$ - ${}^3\text{He}$  system was found in agreement with experiments.

As for the experimental status of eta mesic states, some measurements which give a positive indication of the existence of  $\eta$ -mesic states have been reported in literature. One such experiment was performed by the TAPS collaboration [45] on the photo-production of  $\eta$  on  ${}^3\text{He}$ , namely,  $\gamma {}^3\text{He} \rightarrow \pi^0 p X$ , where one essentially sees the decay of a bound  $\eta$  in  ${}^3\text{He}$  through the  $S_{11}$  resonance. The other one is a bit more recent measurement from COSY on the  $p {}^{27}\text{Al} \rightarrow {}^3\text{He} X$  reaction in a recoil free kinematic set-up [46, 47], where one observes in coincidence with  ${}^3\text{He}$ , the decay of a possible bound

$\eta$ - $^{25}\text{Mg}$  state, again, through the  $S_{11}$  resonance. A detailed account of the experimental status will be given in section 3.

In addition to the above studies of eta-mesic quasibound states, large efforts have also gone in understanding the eta producing reactions which explore the  $\eta$  production vertex in these reactions and the effect of the eta interaction with different nuclei in the final state. The elementary reaction  $NN \rightarrow NN\eta$  has been studied extensively within boson exchange models which include the exchange of  $\pi$ ,  $\eta$ ,  $\rho$  and  $\omega$  mesons. The opinion regarding the role of these mesons seems to be however divided. In one of the first works [48, 49] and more recent ones [50], the  $\rho$  meson was found to play a dominant role. However, measurements of the analyzing power for the  $\vec{p}p \rightarrow pp\eta$  reaction (with  $\vec{p}$  indicating a polarized proton beam) near threshold [51] and theoretical calculations in [52] up to 10 GeV beam energy do not agree with a  $\rho$  meson dominance. The production of  $\eta$  mesons in other reactions such as the  $pd \rightarrow {}^3\text{He}\eta$ ,  $pd \rightarrow pd\eta$  and  $dd \rightarrow {}^4\text{He}\eta$  has been studied [53, 54, 55, 56, 57, 58, 59, 60, 61, 62] within one-, two- and three-body exchange mechanisms proposed in [40]. A detailed account of these works as well as those on the  $p{}^6\text{Li} \rightarrow {}^7\text{Be}\eta$  reaction [63, 64] and the available measurements [34, 35, 37, 38, 39, 65, 66, 67, 68, 69, 70, 71, 72, 73, 74, 75] will be given in section 4. We note here in passing that though the three body mechanism where the large momentum transfer in the production of the massive  $\eta$  meson is shared between nucleons seems to reproduce the threshold data very well, it fails to reproduce the forward peaks in the angular distributions at high energies and thus remains to be an open problem to be settled in future.

This report is organized as follows. As the  $\eta N$  scattering amplitude plays a pivotal role in all the eta-nucleus studies, we begin by giving a comprehensive account on the present knowledge of the elementary amplitude and the procedures employed to obtain it. A large section after this is dedicated to present an exhaustive account of the experimental and theoretical searches for the existence of the exotic eta-mesic states. Considering the vast amount of literature available, though we will try to provide a complete bibliography, the focus of these sections will be on a few theoretical works representative of each type of formalism. In addition to the studies of eta mesic quasibound states, huge efforts have also gone in understanding the eta producing reactions which explore the eta production vertex in these reactions and the effect of the eta interaction with other nuclei in the final state. The reaction mechanisms used for eta production are usually based on models similar to those used for other mesons such as the pions and kaons. Hence after giving a brief description of all available mechanisms and their success in comparison with data, we shall review their relevance for the eta production reactions near threshold as well as at high energies in Section 4. Since the objective of the eta producing reactions is to finally investigate the eta nucleus interaction in the final state, the next section naturally goes over to discuss the results obtained as compared to data. Here, in Section 5, the focus will be on specific reactions, the theoretical estimates for them and their comparison with data. Finally, after having surveyed most of the existing literature on theoretical predictions

and experimental data, we will try to draw conclusions on the range of the strength of the eta nucleon and hence eta nucleus interaction. These conclusions should help in planning experiments for future investigations in this field.

## 2. $\eta$ -nucleon interaction and scattering amplitude

The most appropriate source of the  $\eta$ -nucleon scattering amplitude should, of course, be the elastic scattering data on it. However, such studies can not be pursued because  $\eta$  beams are not available. The next appropriate way then is to obtain it from the  $\eta$  production reactions like  $\pi N \rightarrow \eta N$  and  $\gamma N \rightarrow \eta N$ , where this information appears in the final state through the interaction of the emerging  $\eta$ -meson with the recoiling nucleon. Detailed experimental information on these reactions exists now as the pion and photon beams are in use over a wide range of energies. The database includes the total and the differential cross sections from threshold to high energies. It also includes some polarization measurements. The older of these data have been reviewed in [76, 77], while the most recent ones are given in [78, 79]. Plotted as a function of beam energy the total pion-nucleon cross section shows a sharp growth above the  $\eta$ -threshold, signalling the opening of the  $\eta N$  channel. The sharp rise in the pion-induced eta cross section is attributed to the broad nucleon resonance,  $S_{11}(1535)$ , which is very close to the  $\eta$ -production threshold at  $\sqrt{s} \simeq 1487$  MeV. It is strongly coupled to both the pion and the eta-meson in the s-wave. The other resonances near the  $\eta$ -threshold are the  $P_{11}(1440)$  and  $D_{13}(1520)$ . However, the coupling of  $D_{13}(1520)$  to the  $\eta N$  channel is very weak (branching ratio  $\Gamma_{\eta N}(1520)/\Gamma_{tot}=0.0023\pm 0.0004$ ) and that of the subthreshold but very broad  $P_{11}(1440)$  undetermined. With increasing energy, the  $D_{13}(1520)$  shows up through an interference with the dominant  $S_{11}(1535)$ .

Near threshold the  $\eta$ -nucleon scattering thus consists of elastic scattering,  $\eta N \rightarrow \eta N$  and the reactive  $\eta N \rightarrow \pi N$  channel. It also has another reactive channel  $\eta N \rightarrow \pi\pi N$  (arising from the  $\pi\Delta$  and  $\rho N$  couplings), but the cross section for it is very small. The  $\eta$ -nucleon scattering length  $a_{\eta N}$ , which is the parametrization of the  $\eta$ -nucleon scattering amplitude at low energies, therefore, is complex. Its imaginary part gives a measure of the reactive content of the cross section. Since through the detailed balance theorem, the  $\eta N \rightarrow \pi N$  cross section can be related to the  $\pi N \rightarrow \eta N$  cross section at an appropriate energy, the imaginary part of  $a_{\eta N}$  can be determined directly by the pion-induced eta production data. In [79] in fact, using this and the optical theorem, a lower limit was set on the value of  $\Im m(a_{\eta N})$  in the following way: The optical theorem gives

$$\Im m(a_{\eta N}) = \frac{q_\eta}{4\pi} \sigma_{\eta N}^{tot} = \frac{q_\eta}{4\pi} (\sigma_{\eta N \rightarrow \pi N} + \sigma_{\eta N \rightarrow 2\pi N} + \sigma_{\eta N \rightarrow \eta N}). \quad (1)$$

Applying the detailed balance theorem to it we get

$$\Im m(a_{\eta N}) = \frac{3q_\pi^2}{8\pi q_\eta} \sigma_{\pi^- p \rightarrow \eta n} + \frac{q_\eta}{4\pi} (\sigma_{\eta N \rightarrow 2\pi N} + \sigma_{\eta N \rightarrow \eta N}), \quad (2)$$

which results in

$$\Im m(a_{\eta N}) \geq \frac{3q_\pi^2}{8\pi q_\eta} \sigma_{\pi^- p \rightarrow \eta n}. \quad (3)$$

Using the recent threshold data [78],  $\sigma_{\pi^-p \rightarrow \eta n}/q_\eta = 15.2 \pm 0.8 \mu\text{b}/\text{MeV}$ , gives

$$\Im m(a_{\eta N}) \geq 0.172 \pm 0.009 \text{ fm}. \quad (4)$$

In the above expressions,  $q_x$  is the centre of mass momentum of the particle  $x$ .

With the real part of  $a_{\eta N}$ , however, this is not the case. The  $\eta N$  channel in the  $\pi N$  elastic scattering shows up as a cusp at the  $\eta$  threshold, from where one can not directly determine the value of the real part of  $a_{\eta N}$ . The difficulty in obtaining  $\text{Re}(a_{\eta N})$  can also be seen from the behaviour of a resonance amplitude as a function of energy. A typical scattering amplitude proceeding through a resonance has a characteristic behaviour that, its real part goes through zero at the resonance position and the imaginary part peaks at the same position. Knowing that the  $\eta N$  scattering at low energies is dominated by the  $S_{11}(1535)$  resonance, the real part of the  $\eta N$  amplitude would go through zero at resonance, making it difficult thereby to determine the precise value of the real part of  $a_{\eta N}$  which receives contributions from non resonant processes.

### 2.1. Phenomenological

The  $\eta N$  scattering amplitude in literature has been obtained mostly phenomenologically by analysing the data on the  $\eta$  producing pion- and gamma-induced reactions,  $(\pi, \eta)$  and  $(\gamma, \eta)$ . Since hadronic and electromagnetic  $\eta$  production processes are different, details of  $\eta N$  scattering extracted from them complement each other. In different analyses, the four channels,  $\gamma N$ ,  $\pi N$ ,  $\pi\pi N$ , and  $\eta N$  are included and coupled-channels analyses are performed. In all calculations efforts are always made to include as broad a database as possible and available at the time of a particular calculation. Broadly, these efforts can be classified into two categories. In one class the available data are directly fitted to the T-matrices for the pion elastic scattering and pion- and gamma induced eta production. In another class, a microscopic model is developed to describe the reaction dynamics, and the parameters of this model are fixed by fitting the data. The  $\eta N$  T-matrix is the outcome of these calculations. These  $\eta N$  T-matrices in the first approach are only on-shell. For their off-shell application they need to be extrapolated with some ansatz. The second approach gives the  $\eta N$  T-matrix which has some inbuilt off-shell behaviour. However, because of the inherent fact that the information on the  $\eta N$  T-matrix is an outcome of these calculations, the predicted values of  $a_{\eta N}$  from all these calculations differ from one another. The real part of the  $\eta N$  scattering length is found to have a large spread, from about 0.2 to 1 fm.

The calculations in the first category are often done within the K-matrix approach, where the K-matrix is related to the usual T-matrix by the integral equation [80],

$$T = K - i\pi K\delta(E - H_0)T, \quad (5)$$

where  $H_0$  describes the free motion of the two interacting particles. The K-matrix is Hermitian, and the above transformation ensures that the T-matrix remains unitary. Most detailed K-matrix analyses for the reactions of the present discussion have been carried out in [11, 12, 79]. It is gratifying to see that the latest calculations in [12]



and [79] which use similar inputs give comparable values of  $a_{\eta N} = 0.91 + i 0.27$  and  $1.14 + i 0.31$  fm, respectively. Furthermore, the extracted on-shell  $\eta N$  T-matrix from these calculations is made useful to the few-body eta physics by first writing it in the “effective range expansion” and then extrapolating it to the off-shell region by a simple separable approximation, i.e.

$$T_{\eta N}(q, E, q') = v(q)t_{\eta N}(E)v(q'), \quad (6)$$

with  $v(q) = 1/(1 + q^2\beta^2)$ , where  $\beta$  is the range parameter whose value is not well determined. In [12] it is taken  $= 0.31$  fm. The on-shell t-matrix,  $T_{\eta N}(E)$  is written in terms of the scattering amplitude,  $F_{\eta N}(E)$ , using for the latter the effective range expansion,

$$F_{\eta N}(E)^{-1} + iq_\eta = \frac{1}{a} + \frac{r_0}{2}q_\eta^2 + sq_\eta^4, \quad (7)$$

where  $q_\eta$  is the eta momentum corresponding to energy E.  $t_{\eta N}(E)$  in Eq. (6) is written using another effective range expansion, namely,  $f_{\eta N}(E) + iq_\eta v(q_\eta)^2 = (1/a^s) + (r_0^s q_\eta^2/2) + (s^s q_\eta^4)$  where the parameters  $a^s$ ,  $r_0^s$  and  $s^s$  are related to  $a$ ,  $r_0$  and  $s$ . The scattering amplitude and the t-matrix are related as,  $f_{\eta N}(E) = -\frac{\sqrt{s_{\eta N}}}{2\pi}t_{\eta N}(E)$ . The best set of the “effective range expansion” parameters given in [12] is:  $a=0.91 + i 0.27$  fm;  $r_0 = -1.33 - i 0.30$  fm;  $s = -0.15 - i 0.04$  fm<sup>3</sup>.

In another class of phenomenological studies, again coupled-channel analyses of the four channels,  $\gamma N$ ,  $\pi N$ ,  $\pi\pi N$ , and  $\eta N$  are performed, but the T-matrices are now constructed microscopically in dynamical coupled-channel models of meson production reactions including nucleons and their resonances. The first comprehensive calculation in this class was done in [1]. The authors considered the  $\pi N$  collision channels,  $\pi N \rightarrow \pi N$ ,  $\pi N \rightarrow \pi\pi N$ , and  $\pi N \rightarrow \eta N$ , in the energy region  $\sqrt{s}=1488$  to 1600 MeV. They used a separable interaction model and assumed the reactions to proceed via the  $N^*(1535)$  or  $\Delta(1232)$  isobars. The interaction satisfied a Lippmann-Schwinger (LS) equation

$$T = V + VG_0T \quad (8)$$

with the transition interaction  $V_{ij}$  for channel  $i \rightarrow j$  for a given partial wave  $l$  and for a specific baryon resonance doorway state  $\alpha$  given by

$$\langle p'l | V_{ij}^{\alpha l}(\sqrt{s}) | p \rangle = \frac{h_{i\alpha}^l(p'l)h_{\alpha j}^l(p)}{\sqrt{s} - m_\alpha - \Sigma_{2\pi}^\alpha(\sqrt{s})}, \quad (9)$$

with  $h$  being the vertex function. It had the strength  $g$  of the coupling and the range  $\Lambda$  of off-shell extrapolation as parameters. The full solution of the coupled channel LS equation was given as

$$\langle p'l | T_{ij}^{\alpha l}(\sqrt{s}) | p \rangle = \frac{h_{i\alpha}^l(p'l)h_{\alpha j}^l(p)}{\sqrt{s} - m_\alpha - \Sigma_\pi^\alpha(\sqrt{s}) - \Sigma_\eta^\alpha(\sqrt{s}) - \Sigma_{2\pi}^\alpha(\sqrt{s})}, \quad (10)$$

where  $\Sigma_x$  corresponds to the self energy of the particle  $x$ . The parameters of the model were  $g$ ,  $\Lambda$ , and the bare mass  $m_\alpha$ . These parameters were determined by fitting the  $\pi N$  phase shifts. Cross sections for the  $\pi^- p \rightarrow \eta n$  channel were predicted, which agreed very well with the then available data. The s-wave  $\eta N$  scattering lengths obtained from

the  $\eta N$  scattering amplitude from these calculations were  $0.27 + i 0.22$  fm and  $0.28 + i 0.19$  fm for two available sets of  $\pi N$  data. The  $S_{11}$   $\eta N$  phase shifts were found to have positive values, indicating an attractive interaction.

Another study in the above class, which is quite recent, is a detailed investigation of the  $\pi^- p \rightarrow \eta n$  in Ref. [14]. Unlike [1] this approach fixes all the parameters of the model by fitting all available data on the  $\pi^- p \rightarrow \eta n$  reaction from threshold up to total centre-of-mass energy of about 2 GeV. Constraints on the model parameters from the  $\pi N$  elastic scattering are incorporated from the earlier studies of this reaction by this group. The meson baryon (MB) channels included in the studies are  $\pi N$ ,  $\eta N$ ,  $\pi\Delta$ ,  $\rho N$ , and  $\sigma N$ . The MB transition amplitudes in each partial wave is written as a sum of the background term and a resonance term. The former is taken energy independent and the latter is taken to have the usual resonance structure with the  $N^*$  propagator,  $D_{ij}(E)$ , with the associated resonance self-energy, sandwiched between the dressed vertex functions,  $\Gamma_{MB \rightarrow N^*}$ 's. The calculations include nine nucleon resonances, though the final results of the calculations show that the dominant contribution to the  $\pi^- p \rightarrow \eta n$  reaction comes from the  $S_{11}(1535)$  resonance. This paper presents the t-matrix for each channel in all partial waves. The value of the scattering length from the calculated s-wave  $\eta N$  T-matrix comes out to be  $a_{\eta N} = 0.30 + i 0.18$  fm. It is very interesting to note that this value agrees very closely with the value obtained about two decades back in [1] using a similar theoretical framework (presented in the previous paragraph).

## 2.2. Theoretical

Theoretical studies have also been done in literature in the framework of chiral perturbation theory ( $\chi$ PT) [15, 81, 82].  $\chi$ PT is an effective field theory which maintains the basic symmetries of QCD. It describes well the interaction between the pseudoscalar ( $J^\pi = 0^-$ ) mesons and the ground state baryon octet in an almost parameter free way. The transition interaction,  $V_{ij}$  between different meson-baryon channels in the lowest order chiral Lagrangian is given by

$$V_{ij} = -C_{ij} \frac{1}{4f_i f_j} (2\sqrt{s} - M_i - M_j) \times \sqrt{\frac{M_i + E_i(\sqrt{s})}{2M_i}} \sqrt{\frac{M_j + E_j(\sqrt{s})}{2M_j}} \quad (11)$$

where  $E_i(E_j)$  is the energy of the incoming (outgoing) baryon and  $M$  denotes the mass of the baryon.  $f_x$  is the weak decay constant of the meson  $x$ .  $C_{ij}$  is a fixed constant for each transition, reflecting the SU(3) symmetry. The scattering matrices for different channels are obtained by solving the coupled-channels Bethe-Salpeter equations. Various meson baryon channels (with  $0^-$  mesons and  $1/2^+$  octet baryons) which couple to strangeness  $S=0$  are  $\pi^- p$ ,  $\pi^0 n$ ,  $\eta n$ ,  $K^+ \Sigma^-$ ,  $K^0 \Sigma^0$  and  $K^0 \Lambda$ . The values of the scattering length,  $a_{\eta N}$  obtained in this approach in [15, 81, 82] are  $0.20 + i 0.26$  fm,  $0.26 + i 0.25$  fm and  $0.18 + i 0.42$  fm, respectively.

Finally, we conclude that the best possible calculations using different models and including all available experimental data have been done to obtain the  $\eta N$  scattering

amplitude. Nevertheless, no definite value for the  $\eta N$  scattering length is obtained. There exists a large spread [12, 79, 83] in the values. This happens essentially because of the inherent nature of the problem that  $a_{\eta N}$  can not be extracted directly from the experimental data. We also observe that, in general, the values of  $a_{\eta N}$  coming from theoretical models, like  $\chi$ PT and microscopic phenomenological models tend to be smaller than those obtained phenomenologically from the experimental data directly. A table of all values of  $a_{\eta N}$  obtained until 2002 can be found in [83]. Apart from these and the ones mentioned in the discussions above, there exist calculations with large values such as  $0.991 + i 0.347$  fm [84],  $1.03 + i 0.49$  fm [85] and a rather small  $a_{\eta N} = 0.41 + i 0.26$  fm [86].

### 3. Searches for unstable eta-mesic nuclei

The existence of an eta-mesic nucleus, i.e., a quasibound state of the  $\eta$  meson and a nucleus was predicted due to the attractive nature of the  $\eta N$  interaction. Since its first mention in 1986, several experimental and theoretical searches have been performed for light as well as heavy eta-mesic nuclei. The experimental searches involve the production of  $\eta$  mesons and hence signals for the existence of eta-mesic states via their possible decay modes and final state interactions of eta mesons with nuclei. The theoretical works concentrate on the calculation of the eta-nucleus elastic scattering amplitudes and the solutions with  $\eta$ -nucleus potentials using different approaches. Possible signals from experiments and the conclusions drawn from theoretical works will be discussed in the subsections below.

#### 3.1. Experimental searches

Due to the attractive  $\eta N$  interaction and the proximity of its threshold to the mass of the  $N^*(1535)$  resonance, the  $\eta$ -nucleus interaction can be considered as a series of excitations and decays of  $N^*(1535)$  on the different constituent nucleons, which eventually decays to the  $\pi N$  channel, as shown in Figure 1. The strategy of the experiments looking for  $\eta$ -mesic nuclei is to focus on the  $\pi N$  pair coming from the  $N^*(1535)$  resonance decaying in the nucleus.

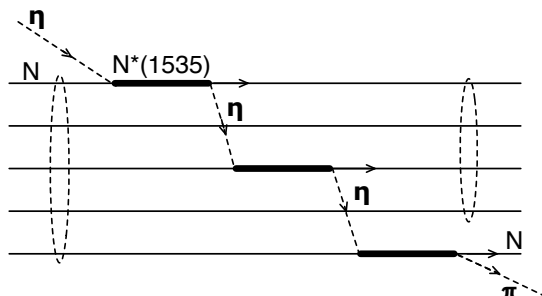


**Figure 1.** Diagrammatical representation of a series of excitations and decays of the  $N^*(1535)$  resonance in the nucleus.

The first experimental search of the  $\eta$ -nucleus bound states [5] was performed at the Brookhaven National Laboratory (BNL) by studying pion collisions with lithium, carbon, oxygen and aluminium but the results turned out to be negative. A few years later another attempt to find these exotic states was made at the Los Alamos Meson Physics Facility (LAMPF) [87] by investigating the process:  $\pi^+ {}^{18}\text{O} \rightarrow \pi^- {}^{18}\text{Ne}$  by varying the beam energy from 350-440 MeV, for the momentum transfer ranging from 0-210 MeV. This experimental search for an  $\eta$ -mesic state in a double charge exchange (DCE) reaction was motivated by an earlier work of Haider and Liu [88] where the authors studied the  ${}^{14}\text{C} (\pi^+, \pi^-) {}^{14}\text{O}$  reaction theoretically and predicted a resonance structure in the excitation function of this reaction at a pion kinetic energy of 419 MeV. For pion beam energies of around 400 MeV, the DCE reaction can proceed in a nucleus via the  $\pi^+ \rightarrow \pi^0 \rightarrow \pi^-$  process (where  $\pi^+ n \rightarrow \pi^0 p$  is followed by  $\pi^0 n \rightarrow \pi^- p$ ) as well as the  $\pi^+ \rightarrow \eta \rightarrow \pi^-$  process. The  $\eta$  can either be in the continuum or in a strongly bound  $\eta$ -nuclear state. They showed that the DCE amplitude associated with the bound  $\eta$  possessed a resonance structure with a narrow width ( $\sim 10$  MeV). Thus an  $\eta$ -nucleus state could act as a doorway state for the  $(\pi^+, \pi^-)$  reaction channel. The situation is somewhat analogous to the appearance of a resonance structure due to compound nucleus formation in low energy nuclear reactions.

The poor statistics in the LAMPF experiment, however, did not allow to conclude more than a weak affirmation of the presence of a structure near the eta threshold. Since then several experiments have been made in different laboratories studying different kinds of eta producing reactions and some experiments claim to have found  $\eta$ -mesic nuclei. In this subsection we will review the different strategies followed in the previous investigations and the results obtained in the same, as well as the new upcoming experiments and their assets.

*3.1.1. Eta meson production in proton induced reactions* Eta production with proton beams scattered on different light targets ( $p$ ,  $d$ ,  ${}^3\text{He}$ ) has been studied experimentally and the resulting data in all these processes show sharply rising amplitudes as the energy approaches the threshold region. This is an indication of the strong attractive  $\eta - A$  interaction and can be related to the formation of a quasibound state in these systems.

The reaction which has been studied most extensively is  $p d \rightarrow {}^3\text{He} \eta$ . The oldest data set on this reaction is available from the Laboratoire National Saturne, Saclay [65]. This study involved a measurement of the  $p d \rightarrow {}^3\text{He} \eta$  reaction corresponding to  $\eta$ -production at very backward angles and at beam energies ranging from 0.92 GeV to 2.6 GeV. Interestingly, the measured cross sections turned out to be comparable to that of the  $p d \rightarrow {}^3\text{He} \pi^0$  reaction. Such large cross sections were not expected since the  $p d \rightarrow {}^3\text{He} \eta$  reaction involves much larger momentum transfer (see Figure 2 for a comparison of the momentum transfer as a function of beam energy for these two reactions). It can be seen from Figure 2 that the momentum transfer for the  $p d \rightarrow {}^3\text{He} \eta$  reaction (solid line) is about 900 MeV and for the  $p d \rightarrow {}^3\text{He} \pi^0$  reaction (dashed line) is about 400 MeV at the respective thresholds.

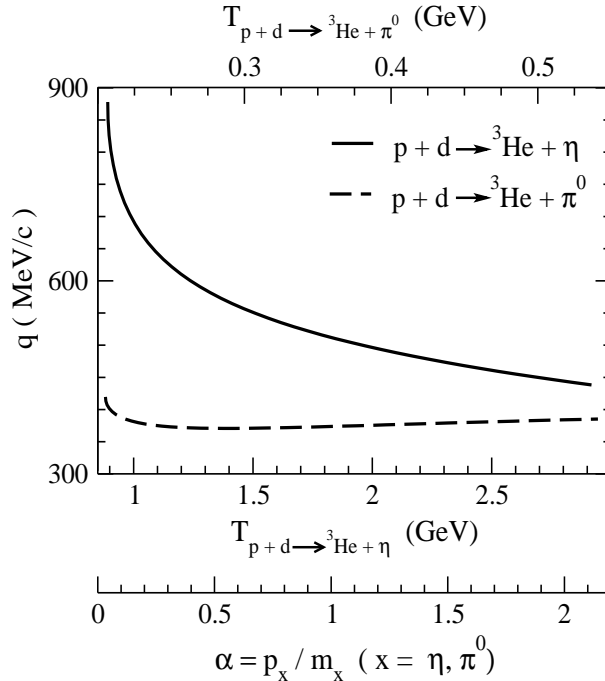


**Figure 2.** A comparison of the momentum transfer involved in the  $p d \rightarrow {}^3\text{He} \eta$  (solid line) and the  $p d \rightarrow {}^3\text{He} \pi^0$  (dashed line and upper scale) reaction as a function of corresponding beam energies. The variable,  $\alpha$ , has been defined such that there exists a common scale for the two reactions.

Another set of measurements on the same reaction [34] was later made at the same laboratory which focused on energies very close to threshold. The  $p d \rightarrow {}^3\text{He} \eta$  cross sections were measured at eight different proton energies from 0.2 to 11 MeV above threshold. Apart from being in agreement with the observation of the previous experiment regarding the surprisingly large cross sections, the experimental data in this region showed that the squared-amplitude decreased nearly by a factor of four within this small energy region, which corresponds to an increase in the  $\eta$ - ${}^3\text{He}$  center of mass momentum by about 75 MeV/ $c$ . The forward-backward asymmetry was negligible indicating that the angular distributions were isotropic in the center of mass system. In other words, the final state particles were found to be produced in the s-wave. Similar features were also found in the data for the  $p n \rightarrow d \eta$  [89] and  $p d \rightarrow p d \eta$  [70] reactions. The squared amplitudes and the total cross section data for these three reactions, in the threshold region, are shown in Figs. 3 and 4 as a function of the excitation energy  $Q = E_{\eta A} - M_\eta - M_A$ , where  $E_{\eta A}$ ,  $M_\eta$ ,  $M_A$  refer to the total energy of the  $\eta$ -nucleus system, the mass of the  $\eta$ -meson and the mass of the nucleus, respectively. Different data sets in Figure 3 have been multiplied by arbitrary factors for the sake of comparison and it can be seen from this figure that the slope of the different squared amplitudes of  $\eta$ -light nuclei is very similar. The sharp structure of the amplitudes near threshold is a clear manifestation of the strong  $\eta$ -nucleus final state interaction which hints towards the existence of possible quasi bound states in such systems. Assuming the dominance

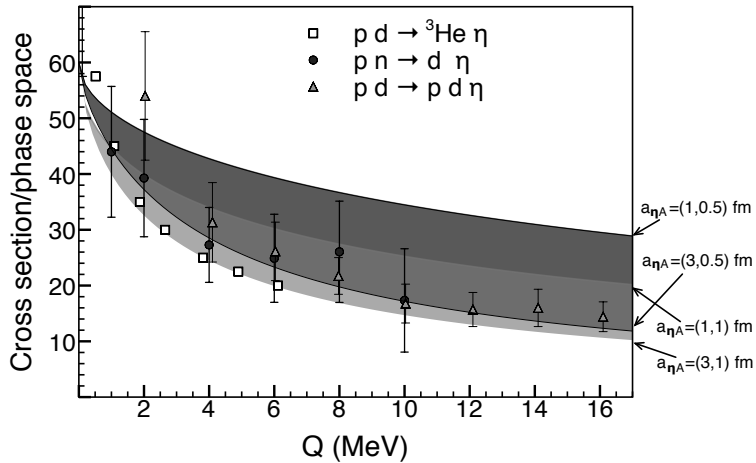


**Figure 3.** Squared amplitude data on the  $p d \rightarrow {}^3\text{He } \eta$  (empty squares) [34],  $p n \rightarrow d \eta$  [89] (filled circles) and  $p d \rightarrow p d \eta$  (open triangles) [70] reactions as a function of the excitation energy in the  $\eta$ -nucleus system. These amplitudes have been multiplied by arbitrary factors to facilitate a comparison among them. As can be seen, the slope of the three data sets is very similar. The meaning of the the dark and light shaded region is explained in the text.

of the  $\eta - A$  interaction in these processes, the corresponding squared amplitude data is often fitted using the  $\eta - A$  scattering length,  $a_{\eta A}$ , as [90]

$$|F(k)|^2 = \frac{f_B}{|1 - ika_{\eta A}|^2}, \quad (12)$$

where  $k$  is the momentum in the  $\eta - A$  center of mass system and  $f_B$  is a normalization factor which is related to the contribution of the Born amplitude of the reaction. The fitting procedure usually concentrates on reproducing the shape of the data with  $f_B$  being an arbitrary parameter used to reproduce the right magnitude of the data. The fitted value of the  $\eta - A$  scattering length is then used to infer an indirect evidence of the formation of an  $\eta - A$  quasibound state. We show the result of the calculation of Eq. (12) by taking  $1 \leq |\Re\{a_{\eta A}\}| \leq 3$  for  $\Im m\{a_{\eta A}\} = 0.5(1)$  by dark(light) shaded regions (these values lie within the range of  $a_{\eta A}$  extracted in Ref. [91]). It can be seen that a reasonable fit is obtained for larger values of  $a_{\eta A}$ . Notice that Eq. (12) is blind to the sign of the  $\Re\{a_{\eta A}\}$ . Though the above approximation looks promising and is often used in literature, such a fitted value of the eta-nucleus scattering length can be quite misleading. We shall discuss this point in greater detail in Chapter 5.

Furthermore, an indication of the presence of a quasibound/quasiresonant state can be also seen from the total cross section data (shown in Fig 4) which cannot be explained by the phase space of the reactions (shown as solid, dashed and dotted lines for  $p d \rightarrow {}^3\text{He } \eta$ ,  $p n \rightarrow d \eta$  and  $p d \rightarrow p d \eta$  reactions, respectively).

Measurement of the cross sections for the proton induced  $\eta$  production on light targets has been made with more statistics near the threshold region [37, 38, 66, 67, 71]. More data are also being made available at higher energies for these reactions [68, 39].

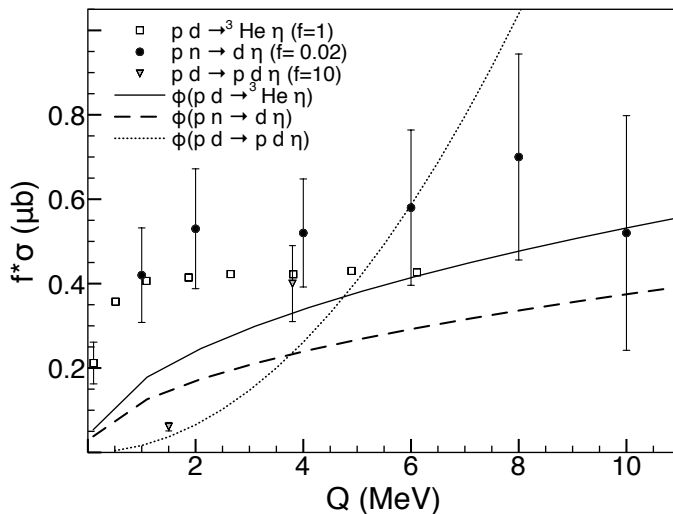


**Figure 4.** A comparison of the total cross sections, multiplied by a factor  $f$  which is given in the figure legends, of the  $p d \rightarrow {}^3\text{He } \eta$  [34],  $p n \rightarrow d \eta$  [89] and  $p d \rightarrow p d \eta$  [70] reactions as a function of the excitation energy ( $Q = \sqrt{s} - \sum_i M_f^i$ , where  $s$  and  $M_f^i$  are the total energy of the system and the mass of the  $i$ th particle in the final state). The lines indicate the phase space,  $\phi$ , for the three reactions.

The data from these experiments show anisotropic angular distributions indicating a possible interplay of higher partial waves in the reaction mechanism at energies farther from the threshold region.

More recently, differential cross section measurements for  ${}^6\text{Li}(p,\eta){}^7\text{Be}$  reaction at 11.28 MeV excess energy have been performed at COSY [73, 75] where the missing mass of the recoiling nucleus  ${}^7\text{Be}$  was measured with the aim of studying the FSI. The total cross section is found to be around  $(8.6 \pm 2.6 \text{ stat.} \pm 2.4 \text{ syst.})$  nb. Compared to this the total cross sections around the same excess energy for  $p d \rightarrow {}^3\text{He } \eta$  and  $d d \rightarrow \alpha \eta$  are around  $(407 \pm 20)$  nb [37] and  $(16 \pm 1.6)$  nb [92, 93], respectively, showing thereby a drastic decrease in the  $\eta$  production cross section with an increase in the target nucleus mass number.

A search for the binding of the eta mesons in heavier nuclei has been done recently at COSY in the  ${}^{27}\text{Al}(p, {}^3\text{He}) p \pi^- X$  transfer reaction [46]. The  ${}^3\text{He}$  is detected at 0 deg. and the beam energy is chosen such that the eta meson goes into the nucleus ( ${}^{25}\text{Mg}$  in this case) with nearly no momentum, increasing thereby its binding probability (recoil free kinematics). Considering that the bound eta meson in the nucleus decays through the  $\pi p$  channel, a triple coincidence is performed in the experiment, where  $p \pi^-$  going in a cone around back to back are measured in coincidence with the  ${}^3\text{He}$  nucleus having missing mass around 550 MeV. This study has led to the finding of a peak structure around 13 MeV with a half width around 5 MeV. This has been attributed to an eta-nucleus bound state in  ${}^{25}\text{Mg}$ . An upper limit on the total cross section for this channel has been fixed in this experiment around 0.5 nb.

A theoretical analysis of the above data has been done very recently, which

strengthens this conclusion (discussed further in Section 3.2.2.). For an overview of the experiments planned at COSY, see Ref. [94].

*3.1.2. Photoproduction and quasibound states* Almost a decade after the studies reported in Refs [5, 87], very conclusive results regarding a clear evidence of an  $\eta$ -mesic nucleus were released from the Mainz Microtron facility (MAMI) [45], where the  $\eta$ -meson was claimed to form a quasibound resonance with a nucleus as light as  ${}^3\text{He}$ . The inclusive cross section for the  $\gamma {}^3\text{He} \rightarrow \eta X$  reaction was measured with the beam energy ranging from threshold to 820 MeV and a resonant structure was found above the  $\eta$  production threshold in the coherent  $\gamma {}^3\text{He} \rightarrow \eta {}^3\text{He}$  cross sections while a peak was seen slightly below the threshold in the  $\pi^0 p$  decay channel. The mass and width of the resonance extracted from these cross sections were reported to be  $[(-4.4 \pm 4.2) - i(25.6 \pm 6.1)]$  MeV. These results are in striking coincidence with those reported in Ref. [41] for small  $\eta N$  scattering lengths, where a possibility of the existence of the  $\eta$ - ${}^3\text{He}$  quasibound state was studied by calculating the Wigner's time delay method using the amplitudes obtained by solving the few body equations for the system. However, this work suffered from the presence of a pole near the threshold which refrained the authors from making strong claims. This work was revisited and a more refined investigation was later made [44] by subtracting the singularity close to threshold. This led to the finding of the existence of  $\eta$ - ${}^3\text{He}$  quasibound to quasivirtual states when the  $\eta N$  scattering lengths were varied from small to large values ( $a_{\eta N} = (0.28, 0.19)$  fm and  $(0.88, 0.41)$  fm which correspond to  $a_{\eta {}^3\text{He}} = (1.16, 0.88)$  fm and  $(2.14, 5.71)$  fm respectively). A more detailed discussion of these calculations will be presented in the next subsection.

However, soon after the release of Ref. [45] a critical comment on the same was published [95] which analysed the  $\gamma {}^3\text{He} \rightarrow \pi^0 p X$  data of Ref. [45] and it was shown that the data was more compatible with the formation of a virtual  $\eta$ - ${}^3\text{He}$  state rather than with a bound state if the corresponding scattering length was assumed to be  $a_{\eta {}^3\text{He}} = (\pm 4, 1)$  fm or  $(0, 3.5)$  fm. The comment was followed by a reply from the experimental group at MAMI [96] where a more refined binning of the data was done. This led to results similar to Ref. [45] and it was concluded that a better statistics would lead to a more unambiguous interpretation. To resolve the issue, a measurement of the cross sections for the coherent  $\gamma {}^3\text{He} \rightarrow \eta {}^3\text{He}$  reaction was repeated [97] with better statistics and by measuring the  $\eta \rightarrow 2\gamma$  as well as  $\eta \rightarrow 3\pi^0 \rightarrow 2\gamma$  decay channels, in order to have better control on the systematic uncertainties. The latter channel was not measured in Ref. [45]. Unfortunately, this more refined study did not lead to more conclusive results. In fact the peak found in Ref. [45] was reproduced in this new experiment but it was found that the peak cannot be attributed to the existence of a resonance unambiguously since it can be explained as an artifact arising from the quasifree pion production background [98].

The photoproduction of  $\eta$ -mesic nuclei has also been studied on  ${}^{12}\text{C}$  at the Lebedev Physical Institute [99] and a lowering of the mass of the  $S_{11}$  resonance has been found in the  $\pi^+ n$  spectrum when the relative angle between the two particles is



180<sup>0</sup>. This has been interpreted as the indication of the formation of an  $\eta$ -mesic nucleus. Photoproduction of the  $\eta$ -meson is also being studied on lighter nuclei at other laboratories [100].

Finally, it should be mentioned that production of the  $\eta$ -mesons is also planned at the DAΦNE facility through the radiative decays of the  $\phi$  mesons [101], with one of the motivations being finding the  $\eta$ -mesic nuclei.

*3.1.3. Eta production with pion beams* In spite of the failure of the earlier experimental searches of  $\eta$ -mesic systems with pion beams at the BNL and LAMPF facilities [5, 87], a proposal to study the pion induced  $\eta$  production on the <sup>7</sup>Li and <sup>12</sup>C targets has been made recently at J-PARC [98]. However, in contrast with the previous investigations [5, 87], there are plans to carry out these experiments within the recoilless kinematics and by demanding an exclusive measurement (like the studies at MAMI and COSY [45, 46]). The beam momentum for these experiments is planned to vary in the range 0.7-1 GeV in order to produce recoilless  $\eta$ -mesons [102]. Furthermore, in order to deduce the possible background from the quasifree production (without excitation of the  $N^*(1535)$  resonance in the medium) of  $\pi^- p$  pair present in the corresponding data, it is planned to measure the cross sections for the  $\pi^+ d \rightarrow p p \eta$  reaction also.

Before ending the discussions on the experimental investigation of  $\eta$ -mesic nuclei, it should be mentioned that  $\eta$  production has also been measured in the  $d d \rightarrow \alpha \eta$  [92, 93] reaction. However, the finding of a  $\eta - \alpha$  quasibound state was not confirmed in these studies.

This discussion can be summarized by stating that some of the existing experimental studies do claim the existence of  $\eta$ -mesic nuclei. However, none of these results have been confirmed by other independent experiments. Many new experiments are planned which promise better statistics and less ambiguity from the background, which in turn will help in making more definitive conclusions regarding the existence of  $\eta$ -mesic nuclei in future.

### *3.2. Theoretical studies*

The theoretical approaches used in the search for the existence of quasibound states of eta mesons and nuclei can be broadly classified into two categories: ones using models based on few body equations for systems of eta mesons and 2 to 4 nucleons and others based on optical potentials for the search of heavy eta-mesic nuclei. In what follows, we shall discuss the findings of the works representative of each category separately. The existence of a quasibound state in these works is confirmed by the occurrence of an S-matrix pole in the complex momentum plane, Argand plots of scattering amplitudes or prominent peaks in time delay. The interesting features of the time delay method which can be used as a complementary tool for locating resonances, quasivirtual and quasibound states will also be discussed below. In Figure 5 we show the location of the poles of the various states in the complex planes to clarify the notation used in

this report. The physical and unphysical sheets correspond to  $\Im m p > 0$  and  $< 0$  respectively.

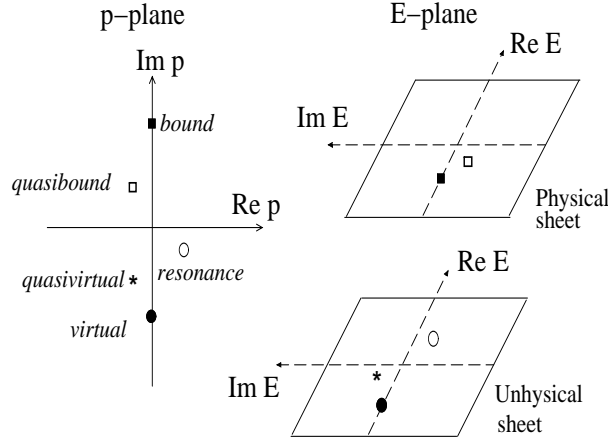


**Figure 5.** Positions of the poles in the complex energy and momentum planes corresponding to bound, virtual, resonant, quasivirtual and quasibound states.

*3.2.1. Few body equations and unstable states of light nuclei* One of the first predictions for light eta-mesic nuclei using few body equations was made by T. Ueda [25]. Since the  $S_{11}$  resonance decays prominently to  $\pi N$  or  $\eta N$ , the author assumes that the  $\eta NN$  system couples necessarily to the  $\pi NN$  system. The three body equation for the amplitude  $X_{\alpha\beta}$  is written as

$$X_{\alpha\beta} = Z_{\alpha\beta} + \sum_{\mu,\nu} Z_{\alpha\mu} \tau_{\mu\nu} X_{\nu\beta} \quad (13)$$

where  $Z$  and  $\tau$  are given by form factors of separable input potentials and the free three body Green's functions [103].  $Z_{\alpha\beta}$  is the particle rearrangement term between particle channels  $\alpha$  and  $\beta$  and  $\tau_{\mu\nu}$  is the propagation term with a spectator particle and an interacting pair in the intermediate channel. Concentrating on isospin 0 and  $J^\pi = 1^-$ , the author considers the coupled  $\eta NN - \pi NN$  system and evaluates the  $\eta d$  scattering amplitude. The input two-body interactions involve the  $\pi N$  potential in the  $P_{11}$  state (though the Roper resonance is ignored),  $NN$  in  ${}^3S_1$ - ${}^3D_1$  state and the  $\pi N \rightarrow \eta N$  potential in the  $S_{11}$  state. A pole structure corresponding to a quasibound state is observed in the amplitude at  $\Re E_\eta = -2$  MeV and  $\Im E_\eta = -10$  MeV.

Following this prediction, a few years later Rakityansky et al. [32] investigated the possibility of forming  $\eta d$ ,  $\eta$ - ${}^3\text{H}$ ,  $\eta$ - ${}^3\text{He}$  and  $\eta$ - ${}^4\text{He}$  states using few body equations. Within a finite rank approximation (FRA), i.e., retaining the interacting nucleus in its ground state, they studied the movement of the poles of the elastic  $\eta$ -light nucleus scattering amplitudes. The  $\eta$ -nucleus transition matrix at any complex energy  $z$  was evaluated by solving the integral equation

$$T(\vec{k}', \vec{k}, z) = \langle \vec{k}', \psi_0 | \sum_{i=1}^A T_i^0(z) | \vec{k}, \psi_0 \rangle \quad (14)$$

$$+ \epsilon_0 \int \frac{d^3 k''}{(2\pi)^3} \frac{\langle \vec{k}', \psi_0 | \sum_{i=1}^A T_i^0(z) | \vec{k}'', \psi_0 \rangle}{\left(z - \frac{k''^2}{2\mu}\right) \left(z - \epsilon_0 - \frac{k''^2}{2\mu}\right)} T(\vec{k}'', \vec{k}, z)$$

where

$$\langle \vec{k}', \psi_0 | \sum_{i=1}^A T_i^0(z) | \vec{k}, \psi_0 \rangle = \int d^{3(A-1)} r |\psi_0(\vec{r})|^2 \sum_{i=1}^A T_i^0(\vec{k}', \vec{k}; \vec{r}; z). \quad (15)$$

$T_i^0(\vec{k}', \vec{k}; \vec{r}; z)$  is obtained by solving another integral equation, namely,

$$T_i^0(\vec{k}', \vec{k}; \vec{r}, z) = t_i(\vec{k}', \vec{k}; \vec{r}, z) + \int \frac{d^3 k''}{(2\pi)^3} \frac{t_i(\vec{k}', \vec{k}''; \vec{r}, z)}{z - \frac{k''^2}{2\mu}} \sum_{j \neq i} T_j^0(\vec{k}'', \vec{k}; \vec{r}, z) \quad (16)$$

where  $t_i(\vec{k}', \vec{k}; \vec{r}, z) = t_{\eta N}(\vec{k}', \vec{k}, z) \exp[i(\vec{k} - \vec{k}') \cdot \vec{r}]$  with  $t_{\eta N}(\vec{k}', \vec{k}, z)$  being the off-shell  $\eta N$  amplitude. This amplitude is written using a separable form and assuming the dominance of the  $S_{11}(1535)$  resonance. The input  $\eta N$  scattering length,  $a_{\eta N}$  was varied and complex poles corresponding to quasibound states of  $\eta d$ ,  $\eta$ - $^3\text{H}$ ,  $\eta$ - $^3\text{He}$  and  $\eta$ - $^4\text{He}$  were found for  $\Re a_{\eta N}$  in the range [0.27, 0.98] fm. The above formalism was later used to study the effects of the final state interactions in  $\eta$  producing reactions such as the  $pd \rightarrow pd\eta$ ,  $pd \rightarrow ^3\text{He} \eta$  and  $p^6\text{Li} \rightarrow ^7\text{Be} \eta$  [58, 59, 60, 61, 62].

A more rigorous treatment of the  $\eta d$  amplitude using the Alt-Grassberger-Sandhas (AGS) equations was carried out in [104] using various values of the input  $\eta N$  scattering length. The exact AGS results were compared with the approximate calculations involving FRA and multiple scattering theory (MST) [105]. It was found that both MST and FRA fail to give the  $\eta d$  scattering length as obtained from the exact AGS calculations in the case of a strong  $\eta N$  interaction (i.e.,  $\Re a_{\eta N} > 0.5$  fm) while for small values of  $\Re a_{\eta N}$  these methods work reasonably well. A three body resonant state near the  $\eta d$  threshold was found in [106] by the same authors using AGS equations. The resonance moved toward the  $\eta d$  threshold when  $\Re a_{\eta N}$  was increased and turned into a quasibound state at  $\Re a_{\eta N} \simeq 0.7 - 0.8$  fm depending on the choice of  $\Im a_{\eta N}$ .

Running counter to all the earlier claims of  $\eta d$  quasibound states, a relativistic three body Faddeev calculation performed in [26, 27] did not find any such state. The authors claimed the existence of quasivirtual states only which moved farther away from threshold with decreasing values of  $\Re a_{\eta N}$ . The authors attribute the difference in their conclusions as compared to earlier works to be due to the difference in the treatment of the two-body interactions which enter as an input to the three-body calculations. Details of the differences can be found in [27, 28]. In [26] a parametrization of the  $\eta d$  amplitude using the effective range formula was also provided. Using this parametrization, it was later shown in [41] that the author in [26] had indeed missed a pole at -17 MeV corresponding to a quasibound state of the  $\eta d$  system using model 0 in that work. Thus the calculation in [26] did support a quasibound  $\eta d$  state though quite away from threshold. We conclude this discussion by mentioning yet another Faddeev approach [107] which was used to evaluate the  $\eta d$  and  $K^- d$  scattering lengths and ruled out the existence of  $\eta d$  quasibound states.

*3.2.2. Optical potential approaches for heavy  $\eta$ -mesic nuclei* In this category two classes of approaches exist, semimicroscopic and fully microscopic. The first class includes using the “ $t\rho$ ” approximation to the  $\eta$ -nucleus optical potential, and the second class includes the QCD based unitarized  $\chi PT$  and the quark-meson-coupling (QMC) construction of the  $\eta$ -nucleus potential. Both the approaches then use these potentials in the Schrödinger or Klein-Gordon equation and search for the bound states.

Let us start with the optical potential approach of Haider and Liu which was introduced in 1986 [2, 3] and led to the prediction of  $\eta$ -mesic states with mass number  $A > 10$ . In a later work [20] the authors used a similar formalism to perform an exploratory study of the effects of the off-shell  $\eta N$  interaction and limitations of approximations using on-shell  $\eta N$  scattering lengths. Here we briefly describe the theoretical framework used in [20] and go on to discuss some interesting consequences drawn in this work. The complex energy eigenvalue  $-|\epsilon|-i|\Gamma|/2$  of an eta-nucleus quasibound state in this work is calculated by solving the momentum space three dimensional integral equation

$$\frac{\vec{k}'^2}{2\mu}\psi(\vec{k}') + \int d\vec{k} \langle \vec{k}' | V | \vec{k} \rangle \psi(\vec{k}) = E\psi(\vec{k}'). \quad (17)$$

Here  $\langle \vec{k}' | V | \vec{k} \rangle$  are momentum space matrix elements of the  $\eta$ -nucleus optical potential  $V$  with  $\vec{k}$  and  $\vec{k}'$  denoting the initial and final  $\eta$ -nucleus relative momenta respectively. Eq. (17) is covariant and leads to the advantage that  $V$  can be related to the elementary  $\eta N$  process by unambiguous kinematical transformations (see Ref. [29] in [20]). The first order microscopic  $\eta$ -nucleus optical potential has the form

$$\begin{aligned} \langle \vec{k}' | V | \vec{k} \rangle &= \sum_j \int d\vec{Q} \langle \vec{k}', -\vec{k}' - \vec{Q} | t(\sqrt{s_j})_{\eta N \rightarrow \eta N} | \vec{k}, -\vec{k} - \vec{Q} \rangle \\ &\times \phi_j^*(-\vec{k}' - \vec{Q}) \phi_j(-\vec{k} - \vec{Q}), \end{aligned} \quad (18)$$

where  $\phi_j$  is the nuclear wave function with the nucleon  $j$  having momenta  $-(\vec{k} + \vec{Q})$  and  $-(\vec{k}' + \vec{Q})$  before and after the collision with  $\vec{Q}$  being the Fermi momentum.  $\sqrt{s_j}$  is the total energy in the centre of mass frame of the  $\eta$  and the nucleon  $j$  and is given by

$$s_j = \left[ m_\eta + m_N - |\epsilon_j| - \frac{\vec{Q}^2}{2M_{c,j}} \left( \frac{m_\eta + m_A}{m_\eta + m_N} \right) \right]^2$$

where  $|\epsilon_j|$  is the binding energy of the  $j^{th}$  nucleon and  $M_{c,j}$  the mass of the core nucleus resulting after the removal of nucleon  $j$ . The integration over  $\vec{Q}$  thus requires the knowledge of the amplitude  $t_{\eta N \rightarrow \eta N}$  at subthreshold energies. The authors present the binding energies and widths of the quasibound states of  $\eta$  mesons and  $^{12}\text{C}$ ,  $^{16}\text{O}$ ,  $^{26}\text{Mg}$ ,  $^{40}\text{Ca}$ ,  $^{90}\text{Zr}$  and  $^{208}\text{Pb}$  within the above off-shell calculation.

They also present another calculation within a factorization approximation (FA) where  $t_{\eta N \rightarrow \eta N}$  is taken out of the integral in (17) and evaluated at an ad hoc momentum  $< \vec{Q} >$ . The  $\eta N$  centre of mass energy  $\sqrt{s}$  is assumed to be  $\sqrt{s} = m_\eta + m_N - \Delta$  with  $\Delta$  being an energy shift parameter. Performing calculations for  $\Delta = 0, 10, 20, 30$  MeV, they notice that for  $\Delta = 30$  MeV the FA results come quite close to the full

off-shell calculations. Interestingly, the downward shift parameter  $\Delta$  that fitted the  $\pi N$  scattering data was also found to be around 30 MeV. The downward shift implies that the  $\eta N$  interaction in  $\eta$ -bound state formation takes place at energies about 30 MeV below the free space threshold. Such a shift can lead to a reduction in the  $\eta N$  attraction inside the nucleus and hence models using the  $\eta N$  interaction in free space could actually be overestimating the  $\eta$ -nucleus binding energy.

The optical potential within the FA was recently used [108] to explain the missing mass spectrum obtained in the recoil free transfer reaction  $p(^{27}\text{Al}, ^3\text{He}) \pi p' X$  performed by the COSY-GEM collaboration. The kinematics in this experiment were chosen in order to search for the  $\eta$ -mesic nucleus  $^{25}\text{Mg}_\eta$ . The authors in [108] showed that the observed peak structure occurs due to coherent contributions from processes where an  $\eta$  binds to  $^{25}\text{Mg}$  to form an intermediate  $^{25}\text{Mg}_\eta$  or it emerges as a pion through  $\eta p \rightarrow \pi^0 p$  scattering in  $^{25}\text{Mg}$  without forming a quasibound state. This quantum interference, the authors observe, gives a weaker binding (-8 to -10) MeV as compared to the experimental value of  $(-13.13 \pm 1.64)$  quoted in [46].

Binding energies and widths of quasibound  $\eta$ -mesic nuclei  $^{12}\text{C}$ ,  $^{40}\text{Ca}$  and  $^{208}\text{Pb}$  were calculated in [21] by evaluating the  $\eta$  self energy which is related to the optical potential. Assuming that the  $\eta N$  interaction is dominated by  $N^*(1535)$  the  $\eta$  self energy was written as

$$\Pi(k) = \frac{g_\eta^2 \rho}{\sqrt{s} - M_{N^*} + i(\Gamma(s)/2) - i\Im m \Sigma_{N^*}(k^0, \vec{k}) + \text{Re} \Sigma_N - \text{Re} \Sigma_{N^*}} \quad (19)$$

where  $g_\eta$  is the  $\eta NN^*$  coupling constant,  $\rho$  is the nuclear density,  $M_{N^*}$  the mass of  $N^*(1535)$ ,  $\Gamma(s)$  its free width and  $\Sigma_{N^*}$  the  $N^*$  self energy in the nuclear medium. The optical potential in a finite nucleus was obtained using the local density approximation (LDA). This potential generated quasibound states with very large widths. The authors concluded that it is unlikely that any narrow peaks corresponding to bound eta states in nuclei would be detected experimentally. Another calculation in a similar spirit was done in [22] where the  $\eta$  self energy was calculated in a chiral unitary approach [109]. The quasibound states were once again found to be with the half widths larger than the separation of the levels.

Quark-meson coupling (QMC) model is a mean field description of the nucleus like Quantum Hadrodynamics (QHD), except that the quark substructure of hadrons is explicitly implemented in it. It uses mean-field equations with meson fields explicitly coupling with the quarks in the hadrons, e.g.  $q\bar{q}$  in the bag for the eta meson. These equations are solved self consistently to determine the in-medium quark masses, interacting fields, and eventually the eta meson mass in the nucleus. If we denote this in-medium  $\eta$  meson mass by  $m_\eta^*(r)$ , the eta-nucleus potential is given by  $V_\eta(r) = m_\eta^*(r) - m_\eta(r)$ , where the unstarred mass is the eta mass in free space. This potential includes the effect of  $\eta - \eta'$  mixing. However, the QMC model does not include the imaginary part of the potential consistently. It is introduced from outside assuming a specific form, with its strength as a free parameter. Using this potential, single particle energies for the  $\eta$  are obtained solving the Klein-Gordon equation. The results are given

for several closed shell nuclei and also for  ${}^6\text{He}$ ,  ${}^{11}\text{B}$  and  ${}^{26}\text{Mg}$ . This work concludes that one should expect to find bound states in all these nuclei.

Finally in passing, we mention an interesting work [110] where the  $N^*(1535)$  being the lowest lying baryon with parity opposite to that of the nucleon is viewed as the chiral partner of the latter. It was found that the  $N^*$ - $N$  mass gap decreases in the nuclear medium with increase in density (chiral symmetry restoration) and the calculations in [110] show the existence of two bound eta-nucleus states at about -80 MeV. Other calculations by the same authors based on chiral models can be found in [111].

*3.2.3. Collision times of eta mesons and light nuclei* In [41, 44] the search for quasibound states of light  $\eta$ -mesic nuclei was carried out using an approach based on Wigner's time delay [112, 113]. This method has been applied earlier to characterize hadron resonances [42, 43] at positive energies but was not used to locate quasibound and quasivirtual states. In [41] the usefulness of the method is demonstrated through a pedagogical example of the neutron-proton system where one can also locate the bound and virtual states via time delay plots. The method is then applied to reproduce some quasivirtual  $\eta$ -mesic states already found in literature and predict quasibound states of  $\eta d$ ,  $\eta$ - ${}^3\text{He}$  and  $\eta$ - ${}^4\text{He}$  nuclei. Here we briefly describe the concept of Wigner's time delay and a modification of it which is useful for locating  $s$ -wave states. A rather different approach based on the concept of "dwell time" was introduced by F. T. Smith in 1960 [114].

Wigner showed the phase time delay in single channel elastic scattering  $\tau_\phi(E)$  (where  $E = \hbar^2 k^2 / 2\mu$  is the particle energy and  $\hbar k$  the momentum) to be related to the energy derivative of the scattering phase shift  $\delta_l(E)$  by  $\tau_\phi^l(E) = 2\hbar d\delta_l/dE$ . The time delay in elastic scattering was related to the lifetime of a resonance [42, 43]. With the phase shift in general being given as  $\delta_l \propto E^{l+1/2}$ , the energy derivative  $d\delta_l/dE \propto E^{l-1/2}$  and leads to a singularity near threshold for  $l = 0$ . This problem can be overcome if instead of Wigner's time delay one considers the "dwell time delay" which is a closely related concept [44]. In a tunneling problem in 1-dimension for example, one finds,

$$\tau_\phi(E) = \tau_D(E) - \hbar [\Im m(R)/k] dk/dE, \quad (20)$$

where the first term on the right is the dwell time or time spent inside the barrier and the second term is a self-interference term which arises due to the interference of the incident and reflected waves.  $R$  is the reflection amplitude which in a scattering problem gets related to the  $S$ -matrix.

Starting from (20), replacing  $R = -S$  with  $S$  related to the complex transition matrix in scattering as,  $S = 1 - i\mu k(t_R + it_I)/\pi$ , where  $t_R$  and  $t_I$  are the real and imaginary parts of the  $t$ -matrix respectively and  $\mu$  is the reduced mass of the system, one obtains the 'self-interference' term in terms of  $t$  as,

$$-\hbar[\Im m(R)/k] dk/dE = -\hbar\mu [t_R/\pi] dk/dE. \quad (21)$$

Replacing the low energy behaviour of the reflection amplitude  $R \sim e^{i(\pi-2ak)}$  [44],  $dk/dE = \mu/\hbar^2 k$  and the definition of the complex scattering length  $a = a_R + ia_I$ ,

namely,  $t(E = 0) = -2\pi a/\mu$ , we see that

$$-\hbar [\Im m(R)/k] [dk/dE] \stackrel{k \rightarrow 0}{\simeq} 2 a_R \mu / (\hbar k)$$

and similarly,  $-\hbar \mu [t_R/\pi] [dk/dE] \stackrel{k \rightarrow 0}{\simeq} 2 a_R \mu / (\hbar k)$ . This indeed is also the threshold singularity present in the definition of the time delay in  $s$ -wave collisions near threshold. The real scattering phase shift for  $s$ -waves,  $\delta \rightarrow k a_R$  close to threshold and Wigner's time delay,

$$\tau_\phi(E) = 2 \hbar [d\delta/dE] \stackrel{k \rightarrow 0}{\simeq} 2 a_R \mu / (\hbar k)$$

(note that the dwell time delay  $\tau_D \stackrel{k \rightarrow 0}{\simeq} 0$ ).

In [44] the relation between the dwell and phase time delay in scattering was thus found to be

$$\tau_D(E) = \tau_\phi(E) + \hbar \mu [t_R/\pi] dk/dE. \quad (22)$$

If one starts with the definition of phase time delay in terms of the  $S$ -matrix,  $\tau_\phi(E) = \Re e[-i\hbar (S^{-1} dS/dE)]$  [114] and uses the relation between  $S$  and  $t$  mentioned above, one gets

$$\tau_\phi(E) = \frac{2\hbar}{A} \left[ \frac{-\mu}{2\pi} k \frac{dt_R}{dE} - \frac{\mu^2 k^2}{2\pi^2} \left( t_I \frac{dt_R}{dE} - t_R \frac{dt_I}{dE} \right) - \frac{\mu}{2\pi} t_R \frac{dk}{dE} \right], \quad (23)$$

with  $A = 1 + (2\mu k t_I/\pi) + (\mu^2 k^2 (t_R^2 + t_I^2)/\pi^2)$ . For elastic scattering in the absence of inelasticities, the factor  $A = 1$ . Once the  $t$ -matrix is known, Eq. (22) can be used to evaluate the dwell time delay in elastic scattering. In [41, 44] the above delay times for  $\eta$ -nucleus elastic scattering were evaluated with the objective of locating quasibound states of  $\eta$  mesons and light nuclei. The  $t$ -matrix for  $\eta d$ ,  $\eta$ - $^3\text{He}$  and  $\eta$ - $^4\text{He}$  elastic scattering was constructed using few body equations within the finite rank approximation explained in the previous subsection. In Figure 6 we see one such plot for the time delay in the reaction  $\eta$ - $^3\text{He} \rightarrow \eta$ - $^3\text{He}$ . As discussed above the phase time delay consists of a sharp singularity near threshold. However, after subtracting the singular term one obtains

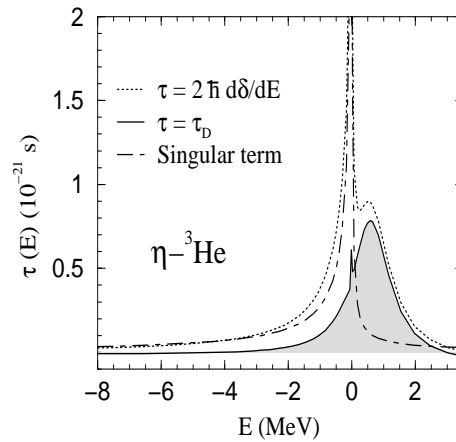


**Figure 6.** Time delay in elastic  $\eta$ - $^3\text{He}$  scattering [44].

**Table 1.** Pole values of eta-mesic light nuclear states

	Complex Pole ( $E, \Gamma/2$ ) in (MeV)	State	Ref.
$\eta d$	$-2 - i 10$	Quasibound	[25]
	$-i 10.317$	Quasibound	[32]
	$28.06 - i 24.976$	Resonance	[32]
	$8.24 - i 4.575$	Resonance	[32]
	$3.73 - i 3.405$	Resonance	[32]
	$i 0.743$	Quasivirtual	[29]
	$-24 + i 27.93$	Quasivirtual	[26]
	$-0.87 + i 0.95$	Quasivirtual	[26]
	$-17.1 - i 17.5$	Quasibound	Missed in [26] noted in [41]
	$-15 - i 20$	Quasibound	[41]
$\eta\text{-}^3\text{He}$	$7.03 - i 13.1$	Resonance	[32]
	$-i 11.15$	Quasibound	[32]
	$0.5 - i 0.65$	Resonance	[44]
	$-5 - i 8, -i 1.95$	Quasibound	[44]
$\eta\text{-}^4\text{He}$	$-4.44 - i 6.37, -i 5.725$	Quasibound	[32]
	$-2 - i 1.75$	Quasibound	[44]

the dwell time delay (Eq. (22)) which appears very clearly with a typical Lorentzian form of a resonance. The curves shown in Figure 6 correspond to an  $\eta N$  scattering length input of  $a_{\eta N} = 0.88 + i 0.41$  fm. Quasibound states in the  $\eta d$  and  $\eta$ -He systems were located by varying the strength of the  $\eta N$  interaction [41]. The authors found that small  $\eta N$  scattering lengths were more favourable for the generation of quasibound states. An example of the  $\eta\text{-}^4\text{He}$  quasibound system with an input  $\eta N$  scattering length of  $0.28 + i 0.19$  fm is shown in Figure 2 in [44]. With  $a_{\eta N} = 0.88 + i 0.41$  fm, a negative time delay peak is obtained. This could correspond to a possible quasivirtual state centered near zero energy as discussed in [41]. A detailed account of these results can be found in [41, 44].

Before ending this section we list in Tables 1 and 2 the pole positions for light and heavy eta mesic states found in literature. In case of heavy nuclei one expects stronger attraction and all the listed states are predictions for quasibound states. The status of the light eta-mesic nuclei is however different and we list the quasibound, quasivirtual and resonant states found so far. Since some papers list several states for varying input parameter sets, we list only some representative values and refer the reader to the original reference in the last column for all values.



Table 2: Quasibound  $\eta$ -mesic states

Nucleus		Pole values in MeV	Ref.
<sup>6</sup> He	1s	-10.7 - <i>i</i> 7.25, -8.75 - <i>i</i> 14.95	[23]
<sup>11</sup> B	1s	-24.5 - <i>i</i> 11.4, -22.9 - <i>i</i> 23.05	[23]
<sup>12</sup> C	1s	-1.19 - <i>i</i> 3.67	[20]
		-9.71 - <i>i</i> 17.5	[22]
		- 5 - <i>i</i> 8, -6 - <i>i</i> 16	[21]
<sup>16</sup> O	1s	-3.45 - <i>i</i> 5.38	[20]
	1p	-32.6 - <i>i</i> 13.35, -31.2 - <i>i</i> 26.95	[23]
		-7.72 - <i>i</i> 9.15, -5.25 - <i>i</i> 19.1	[23]
<sup>24</sup> Mg	1s	-12.57 - <i>i</i> 16.7	[22]
<sup>26</sup> Mg	1s	-6.39 - <i>i</i> 6.6	[20]
		-38.8 - <i>i</i> 14.25, -37.6 - <i>i</i> 28.65	[23]
<sup>27</sup> Al	1s	-16.65 - <i>i</i> 17.98	[22]
	1p	-2.9 - <i>i</i> 20.47	[22]
<sup>28</sup> Si	1s	-16.78 - <i>i</i> 17.93	[22]
	1p	-3.32 - <i>i</i> 20.35	[22]
<sup>40</sup> Ca	1s	-8.91 - <i>i</i> 6.8	[20]
		-14 - <i>i</i> 43, -18 - <i>i</i> 21, -14 - <i>i</i> 11.5	[21]
		-46 - <i>i</i> 15.85, -44.8 - <i>i</i> 31.8	[23]
	1p	-17.88 - <i>i</i> 17.19	[22]
		-3 - <i>i</i> 16.5	[21]
		-7.04 - <i>i</i> 19.3	[22]
2s	-26.8 - <i>i</i> 13.4, -25.2 - <i>i</i> 27.1	[23]	
		-4.61 - <i>i</i> 8.85, -1.24 - <i>i</i> 19.25	[23]
<sup>90</sup> Zr	1s	-14.8 - <i>i</i> 8.87	[20]
		-52.9 - <i>i</i> 16.6, -51.8 - <i>i</i> 33.2	[23]
	1p	-4.75 - <i>i</i> 6.7	[20]
		-40 - <i>i</i> 15.25, -38.8 - <i>i</i> 30.6	[23]
2s	-21.7 - <i>i</i> 13.05, -19.9 - <i>i</i> 26.55	[23]	
<sup>208</sup> Pb	1s	-18.46 - <i>i</i> 10.11	[20]
		-25 - <i>i</i> 47, -27 - <i>i</i> 23.5, -22 - <i>i</i> 12.5	[21]
		-21.25 - <i>i</i> 15.88	[22]
		-56.3 - <i>i</i> 16.6, -55.3 - <i>i</i> 33.1	[23]
	1p	-12.28 - <i>i</i> 9.28	[20]
		-18 - <i>i</i> 45, -21 - <i>i</i> 22, -16 - <i>i</i> 12	[21]
		-17.19 - <i>i</i> 16.58	[22]
		-48.3 - <i>i</i> 15.9, -47.3 - <i>i</i> 31.75	[23]
2s	-2.37 - <i>i</i> 5.82	[20]	

continues on the next page

Nucleus	Pole values in MeV	Ref.
	-10 - $i$ 20, -6 - $i$ 10.5	[21]
	-10.43 - $i$ 17.99	[22]
	-35.9 - $i$ 14.8, -34.7 - $i$ 29.75	[23]
1d	-3.99 - $i$ 6.9	[20]
	-12.29 - $i$ 17.74	[22]
1f	-6.64 - $i$ 19.59	[22]
2p	-3.79 - $i$ 19.99	[22]
1g	-0.33 - $i$ 22.45	[22]

#### 4. Reaction mechanisms for meson production

With the momentum transfer in meson producing reactions being large, there exist certain common features regarding the role of the reaction mechanisms producing pions, eta mesons and kaons. In the sections which follow, we shall discuss the cross section features of proton induced  $\eta$  meson producing reactions and theoretical works which try to explain them. These include the  $pd \rightarrow pd\eta$ ,  $pd \rightarrow {}^3\text{He} \eta$  and the  $p{}^6\text{Li} \rightarrow {}^7\text{Be} \eta$  reactions. The latter can indeed be modelled in terms of the  $pd \rightarrow {}^3\text{He} \eta$  reaction within a cluster model for the nuclei  ${}^6\text{Li}$  and  ${}^7\text{Be}$ . In view of the above, let us start the discussion with the possible reaction mechanisms for the production of  $\eta$  mesons in  $pd$  collisions.

##### 4.1. One, two and three body mechanisms

The need for two- and three-body mechanisms apart from the one-body mechanism for meson production was noticed by Laget and Lecolley [115]. The three-body mechanism in particular is necessary to recover the agreement between theory and experiment for reactions involving  $\eta$  meson production. Due to the large mass of the  $\eta$  (547.85 MeV), the momentum transfer to the residual nucleus is large and is more likely shared by three rather than two nucleons. The one-, two- and three-nucleon graphs for meson production in  $pd$  collisions as discussed in [40, 115] are shown in Figure 7. Note that in the three-body mechanism, the proton interacts in the first step with a nucleon in the deuteron to produce an off-shell meson which in the next step interacts with the other nucleon in the deuteron to produce the on-shell meson in the final state.

Laget and Lecolley found that [40] the one- and two-body mechanisms in the  $pd \rightarrow {}^3\text{He} \eta$  reaction underestimated the experimental cross sections by two orders of magnitude. The role played by this mechanism and its limitations were later discussed in [58]. Though a two-step model (involving the three-body mechanism) did succeed in reproducing the right order of magnitude of cross sections, the forward peaking in the angular distributions at high energies could not be reproduced very well. A similar model was used in [56] to study the  $pd \rightarrow {}^3\text{H} \text{K}^+$  reaction up to beam energies of 3 GeV. The authors found the one- and two-body mechanisms to contribute 2-3

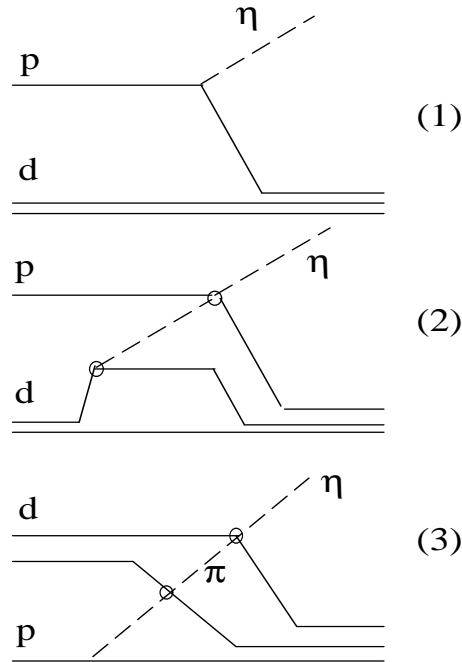


**Figure 7.** The one-, two- and three-body meson exchange graphs for  $\eta$  production in  $pd$  collisions. Exchange graphs arising due to antisymmetrization are not shown here but can be found in [40].

orders of magnitude lesser than the three-body mechanism and produced backward peaked angular distributions (consistent with the findings of [58]). Similar problems in reproducing the angular distributions for the  $p d \rightarrow {}^3\text{He } \omega$  reaction also have been reported in Refs [116, 117].

Finding a mechanism which produces the right order of magnitude of the cross sections as well as the right peaking in the angular distributions remains to be an open question. In subsections 4.2 and 4.3 respectively we shall discuss the threshold and high energy proton induced  $\eta$  production. The theoretical models in 4.2 are two step models whereas 4.3 discusses a meson exchange model which in spite of being a one step model seems to reproduce the data on  $pd \rightarrow {}^3\text{He } \eta$  at high energies well [57]. The reason behind this could be the coherent sum of meson exchange diagrams which is not used in the other approaches or the difference in the nuclear wave functions used. A calculation based on the meson exchange model and using a rigorous few body formalism for the inclusion of the final state eta-nucleus interaction could turn out to be useful in understanding the reaction mechanisms involved in the  $\eta$  producing reactions.

#### 4.2. Proton induced $\eta$ production on light nuclei and cross section features near threshold

The cross sections of reactions such as the  $p d \rightarrow {}^3\text{He } \eta$ ,  $p d \rightarrow p d \eta$  and  $p n \rightarrow d \eta$ , display very similar features as seen in Figs 3 and 4. We saw earlier that the sharp rise near threshold is attributed in literature to the strong  $\eta$ -nucleus

FSI. The production mechanisms for these reactions are based on diagrams discussed in the previous subsection. However, apart from such descriptions, there also exist meson exchange models which are used to describe the  $\eta$  production in  $pN$  collisions [48, 50, 52, 118, 119, 120, 121, 122] and then further applied to  $\eta$  production with  $p$ -nucleus collisions. Such models will be discussed in the next subsection.

In the present subsection, as an example, we briefly discuss the formalism where a two step model is used to produce the  $\eta$ - $^3\text{He}$  system in the  $p d$  collision and where few body equations are solved to include the final state interactions. The same formalism can be used to study the proton (or deuteron) induced  $\eta$  production on other light nuclei [55, 61, 62, 63, 64, 123]. The  $p d \rightarrow p d \eta$  reaction, where, once again the two step model has been used, will be discussed in one of the subsequent sections.

The Born amplitude for the two step process,  $\langle |T_{pd \rightarrow ^3\text{He}\eta}| \rangle$ , can be written as [40, 54, 56, 60, 115]

$$\begin{aligned} \langle |T_{pd \rightarrow ^3\text{He}\eta}| \rangle &= i \int \frac{d\vec{p}_1}{(2\pi)^3} \frac{d\vec{p}_2}{(2\pi)^3} \sum_{int m's} \langle pn | d \rangle \langle \pi d | T_{pp \rightarrow \pi d} | pp \rangle \\ &\times \frac{1}{(k_\pi^2 - m_\pi^2 + i\epsilon)} \langle \eta p | T_{\pi N \rightarrow \eta p} | \pi N \rangle \langle ^3\text{He} | pd \rangle, \end{aligned} \quad (24)$$

where the sum runs over the spin projections of the intermediate off-shell particles and  $k_\pi$  is the four momentum of the intermediate pion. The matrix elements  $\langle pn | d \rangle$ ,  $\langle ^3\text{He} | pd \rangle$ ,  $\langle \pi d | T_{pp \rightarrow \pi d} | pp \rangle$  and  $\langle \eta p | T_{\pi N \rightarrow \eta p} | \pi N \rangle$  can be obtained from Refs [1, 15, 124, 125, 126], for example. The FSI can be incorporated in the formalism by writing the  $\eta$ - $^3\text{He}$  wave function as a sum of the plane wave and the scattered wave as

$$\langle \Psi_{\eta^3\text{He}}^- | = \langle \vec{k}_\eta | + \int \frac{d\vec{q}}{(2\pi)^3} \frac{\langle \vec{k}_\eta | T_{\eta^3\text{He}} | \vec{q} \rangle}{E(k_\eta) - E(q) + i\epsilon} \langle \vec{q} |, \quad (25)$$

where  $T_{\eta^3\text{He}}$  is the T-matrix for  $\eta^3\text{He}$  elastic scattering. In this way, the  $T$ -matrix for the  $p d \rightarrow ^3\text{He} \eta$  process, including the  $\eta^3\text{He}$  interaction, becomes

$$\begin{aligned} T &= \langle \vec{k}_\eta; m_3 | T_{pd \rightarrow ^3\text{He}\eta} | \vec{k}_p; m_1 m_2 \rangle + \\ &\sum_{m'_3} \int \frac{d\vec{q}}{(2\pi)^3} \frac{\langle \vec{k}_\eta; m_3 | T_{\eta^3\text{He}} | \vec{q}; m'_3 \rangle}{E(k_\eta) - E(q) + i\epsilon} \langle \vec{q}; m'_3 | T_{pd \rightarrow ^3\text{He}\eta} | \vec{k}_p; m_1 m_2 \rangle. \end{aligned} \quad (26)$$

The  $\eta$ -light nucleus system constitutes of few particles and hence the corresponding interaction can be obtained accurately by solving few body equations. A more detailed discussion on the importance of solving few-body equations for light systems will be made in Section 5.1. But, in brief, it can be mentioned at this point that the few body equations take into account the multiple off-shell scattering of the  $\eta$ -meson on different nucleons which are bound as a nucleus. Indeed, the  $\eta^3\text{He}$  interaction was obtained by solving few body equations by considering the  $^3\text{He}$  nucleus to remain in its ground state in Refs [31, 32, 33, 58, 59, 60] and the resulting amplitude was used to calculate Eq. (26) in Refs [58, 59, 60].

The squared amplitude for the  $p d \rightarrow ^3\text{He} \eta$  reaction calculated within such a formalism is shown in Figure 8. The squared amplitude obtained by assuming plane

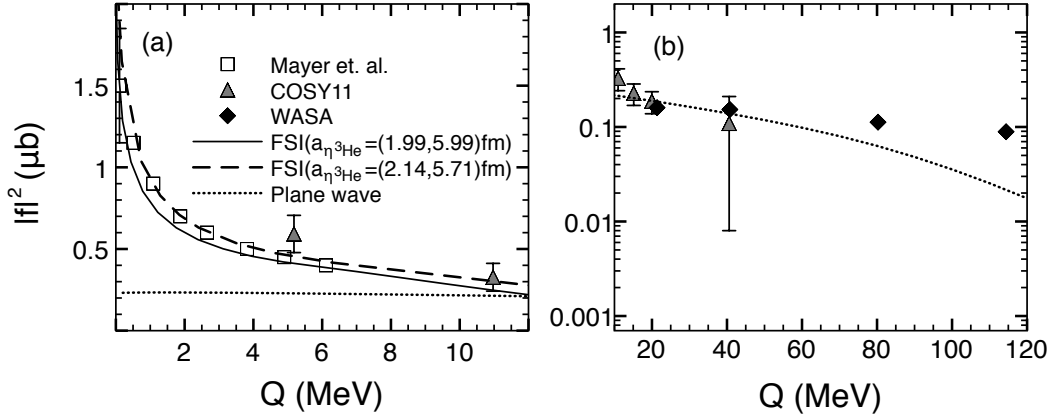


**Figure 8.** The squared amplitude of the  $p d \rightarrow {}^3\text{He} \eta$  reaction for the excitation energies,  $Q(= \sqrt{s} - M_{{}^3\text{He}} - M_\eta) < 12$  MeV is shown in the left panel and for  $10 < Q < 120$  is shown in the right panel. The figure shows data from Refs [34, 66, 68] as empty squares, filled triangles and filled rhombuses respectively. The meaning of the lines [58, 59, 60] is explained in detail in the text.

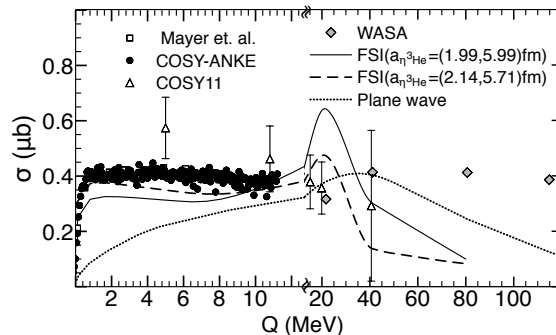
waves for the final state particles is shown by dotted lines in Figure 8. The figure shows that these results cannot explain the sharp structure present in the near-threshold data of Refs [34] (shown by empty squares) and [66] (shown by filled triangles). However, these data in the threshold region can be well reproduced by taking the  $\eta$ - ${}^3\text{He}$  FSI into account as shown by the solid and dashed lines in Figure 8(a). These results have been obtained by incorporating the FSI calculated by solving few-body equations taking two different input  $\eta N$  interactions corresponding to scattering lengths  $a_{\eta N} = (0.75, 0.27)$  fm [127, 128] and  $(0.88, 0.41)$  fm [27], which give the  $\eta$ - ${}^3\text{He}$  scattering lengths to be  $a_{\eta {}^3\text{He}} = (1.99, 5.99)$  fm and  $(2.14, 5.71)$  fm, respectively (for more details on the calculations which lead to the results shown by solid and dashed lines, please look at Refs [58, 59, 60]).

Figure 8(b) shows the data [66] and the plane wave calculation done in Ref. [59, 60] for the squared amplitude of the  $p d \rightarrow {}^3\text{He} \eta$  reaction at higher excitation energies,  $Q > 10$  MeV. It can be seen that the calculation done by assuming plane waves for the final state can explain the data up to  $Q \sim 60$  MeV but starts deviating from the data beyond that. It is possible that a different production mechanism dominates in this energy region. It is important to mention one of the shortcomings of the two-step model here. This model leads to isotropic angular distributions very close to the threshold region but one obtains backward peaked angular distributions at higher excitation energies.

The total cross sections for the  $p d \rightarrow {}^3\text{He} \eta$  reaction can be calculated as

$$\left(\frac{d\sigma}{d\Omega}\right)_{c.m} = \frac{1}{12} \frac{m_p m_d m_3}{(2\pi E_c)^2} \frac{p_c^f}{p_c^i} \sum_{if} |T_{fi}|^2, \quad (27)$$

where  $m_p$ ,  $m_d$ ,  $m_{^3\text{He}}$  are the masses of the proton, deuteron and the  $^3\text{He}$  nucleus, and  $E_c$ ,  $p_c^f$ ,  $p_c^i$  refer to the total center of mass energy and momenta in the final and initial state, respectively. We show the data on the total cross section and the results of its calculations done by using the two-step model for the production mechanism and a solution of the few-body equations for the  $\eta^3\text{He}$  FSI (as done in Refs [58, 59, 60]) in Figure 9. In this figure too, the dotted, dashed and solid lines, respectively, show the results of the calculations done in the plane wave approximation and by taking the FSI into account using two different inputs, as explained above. Once again, the near threshold data seems to get well explained by this model but the agreement between the two becomes poor at relatively higher energies.



**Figure 9.** The total cross sections for the  $p d \rightarrow ^3\text{He} \eta$  reaction. The data from Refs [34, 37, 66, 68] are shown, respectively, by empty squares, filled circles, empty triangles and empty rhombuses. The theoretical curves [59] are discussed in detail in the text.

#### 4.3. Meson exchange model for eta production at high energies

As discussed above, the two-step model describes well the available eta meson production data on the  $pd \rightarrow ^3\text{He} \eta$  reaction near threshold. The angular distributions near threshold are isotropic. At high energies, though the model still reproduces the right order of magnitude of the cross sections [40, 56, 58], it fails to reproduce the forward peaks in the angular distributions. In [58] the authors discussed the limitations of this model in detail and showed that only some ad hoc manipulations of the model such as restricting the intermediate pion to be on shell and to be produced in the forward direction could change the backward peaked  $\eta$  angular distributions in this model to forward ones. This discrepancy in the angular distributions gives rise to the need for investigating models other than the two step model which has been widely used in literature.

In what follows, we shall discuss a model for the  $pd \rightarrow ^3\text{He} \eta$  reaction where the  $\eta$  is produced via the  $pN \rightarrow pN\eta$  reaction. The elementary  $pN \rightarrow pN\eta$  reaction is described within a boson exchange model (BEM) involving the exchange of the  $\pi$ ,  $\eta$ ,  $\rho$  and  $\omega$  mesons. The calculated cross sections over a wide energy range for the  $pp \rightarrow pp\eta$

reaction have been found in this model to agree very well with the measured ones. In the following, therefore, we first give a brief description of the existing BEM descriptions of the  $pp \rightarrow pp\eta$  reaction in literature and then discuss the work which uses the BEM for the  $pN \rightarrow pN\eta$  reaction as an input to describe the  $pd \rightarrow {}^3\text{He} \eta$  reaction.

*4.3.1.  $pp \rightarrow pp\eta$  reaction* BEM based detailed studies of the  $pp \rightarrow pp\eta$  reaction can be found in Refs [48, 50, 52, 119, 120, 121]. All these calculations recognize that the  $\eta N$  interaction is dominated by the  $S_{11}(1535)$  nucleon resonance. Hence, all of them assume that in the  $pp$  collision in the incident channel one of the protons (projectile or the target) gets excited to the  $S_{11}(1535)$  resonance, which then decays to  $\eta p$ , i.e.  $pp \rightarrow NS_{11}(1535) \rightarrow pp\eta$ . The t-matrices corresponding to the projectile and target excitations are called respectively “direct” and “exchange” terms. In the full t-matrix for the process  $pp \rightarrow pp\eta$ , these t-matrices appear as a coherent sum with opposite signs because of the antisymmetry of the proton-proton wave functions, i.e.

$$T(pp \rightarrow pp\eta) = T_D(pp \rightarrow pp\eta) - T_E(pp \rightarrow pp\eta). \quad (28)$$

The choice of the exchanged mesons between the interacting protons in the entrance channel is also guided, to a certain extent, by the dominant decay modes of the  $S_{11}$  resonance. All the calculations thus have a pion-exchange because the  $S_{11}$  resonance strongly couples to a pion in addition to an eta meson. Coupling to a  $\rho$  meson is included because of the large radiative width of the  $S_{11}$  resonance and the vector meson dominance (VMD) in the radiative coupling. Thus all these studies of the elementary reaction,  $pp \rightarrow pp\eta$  include  $\pi + \rho$ -exchange. Refs [50, 52], however, include the exchange of some other mesons too. However, they find that the  $\pi + \rho$ -exchange plays the deciding role. The parameters associated with the coupling and propagation of all these mesons are decided in all the calculations by data on independent relevant processes. Thus, in that sense, the calculations were parameter free. All other couplings being similar, the  $\rho NN^*$  coupling in [52] is different by being  $\gamma_5 \sigma_{\mu\nu}$  from those in the other two studies [48, 50], where it is  $\gamma_5 \gamma_\mu$ . This difference, as we will see later, leads to very different magnitude of the  $\rho$ -exchange contribution to cross sections.

The above calculations also included the final state interaction (FSI) amongst  $p, p$  and  $\eta$  in different ways and to varying degrees. The authors in [48] incorporate the FSI by modifying the  ${}^1S_0$   $pp$  wave only. For this they use the Paris potential at all the energies except near threshold, where they use the Coulomb corrected effective range expansion. These calculations do not include the interaction of the  $\eta$  meson with the protons. The calculated total cross sections are presented up to 3 GeV beam energies. They reproduce the available data, which were very limited, at the time of this calculation. This calculation also found that the  $\rho$ -exchange transition amplitude dominates.

In [52] the FSI is included amongst all three outgoing particles, taking them pairwise, within the Watson-Migdal theory. Here the t-matrix without FSI is multiplied by a sum of three two-body subsystem factors, each one of them described through the

Jost function written in terms of the corresponding effective range expansion parameters and corrected for the Coulomb interaction in the  $pp$  pair. The FSI is included only for  $s$ -wave. The calculated total cross sections agree well with the measured values over a large energy range. The author also finds, in contrast to the findings in [48, 50], that the  $\rho$ -exchange term does not dominate the cross sections. This observation seems to be supported by the recent analyzing power measurements on the  $pp \rightarrow pp\eta$  reaction.

The treatment of the FSI in [50] follows a different approach, given earlier by the same authors in the study of the  $pp \rightarrow n\Delta^{++}$  reaction [129]. The FSI amongst  $pp\eta$  is envisaged to consist of the interaction between  $\eta$  and a proton, and that of this pair and another proton. Since the dominant effect of the former is to excite the  $S_{11}(1535)$  resonance, the  $t$ -matrix for the  $pp \rightarrow pp\eta$  process is decomposed into a  $t$ -matrix for the transition  $pp \rightarrow pS_{11}(1535)$  and the decay probability of  $S_{11}$  to  $\eta p$ . The interaction between  $\eta p$  and the other proton is incorporated using a distorted wave for the  $pS_{11}$  system in the transition matrix. The initial state interaction is also included in this work by using a distorted wave for the  $pp$  wave in the initial state (for details see [50]). Calculated total cross sections in this work are found to agree very well with the measured ones from threshold to high energies. Like in [48] the dominant contribution to the cross section is found to come from the  $\rho$ -exchange.

*4.3.2.  $pd \rightarrow {}^3\text{He} \eta$*  Since the BEM seems to be successful in reproducing the elementary  $\eta$  production data in  $pp$  collisions, it is worth reviewing a model for the  $pd \rightarrow {}^3\text{He} \eta$  reaction based on this input [57]. Though this model appears at a first glance to be quite similar to the one step model discussed in [40, 130], it differs in details and the authors reproduce the right order of magnitude of the  $pd \rightarrow {}^3\text{He} \eta$  cross sections in addition to the forward peaked angular distributions. Let us briefly review this work first and then compare it with other works in literature.

The authors in [57] consider two diagrams corresponding to the excitation of the projectile proton and a nucleon in the target nucleus  ${}^3\text{He}$ . The transition matrix for a typical diagram, Figure 10(a) is written as

$$T_{fi} = \frac{1}{(2\pi)^6} \int d\vec{k}_1 d\vec{k}_2 \psi_{He}(\vec{k}_1, \vec{k}_2) \Gamma_{NN^*\eta}(k_\eta) \\ \times G_{N^*}(\vec{Q}) V_{NN \rightarrow NN^*}(\vec{q}, \omega) \psi_d(\vec{K}),$$

where  $\vec{Q} = 2\vec{k}_\eta/3 + \vec{k}_1$ ,  $\vec{q} = \vec{k}_p - 2\vec{k}_\eta/3$ , and  $\vec{K} = \vec{k}_\eta/3 - \vec{k}_p/2 + \vec{k}_1 + \vec{k}_2$ .  $N^*$  denotes the  $S_{11}(1535)$  resonance.  $G_{N^*}$  and  $\Gamma_{NN^*\eta}(k_\eta)$  denote its propagation and decay vertex into  $N\eta$  respectively. The transition potential  $V_{NN \rightarrow NN^*}(\vec{q}, \omega)$  is written in terms of the vertex functions at the  $xNN$  and  $xNN^*$  vertices ( $x = \pi, \eta, \rho$  or  $\omega$  meson) and the meson propagator. The bound state deuteron and  ${}^3\text{He}$  wave functions are described by the Hulthen and Gaussian wave functions respectively (see [57] for details) and consist only of the  $s$ -wave components. The parameters of the Gaussian wave function are chosen to reproduce the experimental mean square radius of  ${}^3\text{He}$ . The angular distributions were evaluated as in Eq. (27) using the transition amplitude discussed



above. Calculations were done for a beam energy of 88.5 MeV above threshold where data from the GEM collaboration at COSY exist [69]. In these calculations the target and projectile excitations were added with opposite signs, and include the excitation of both, the neutron and proton in  ${}^3\text{He}$ . These results along with the data are shown in Figure 10, and are seen to reproduce them well.

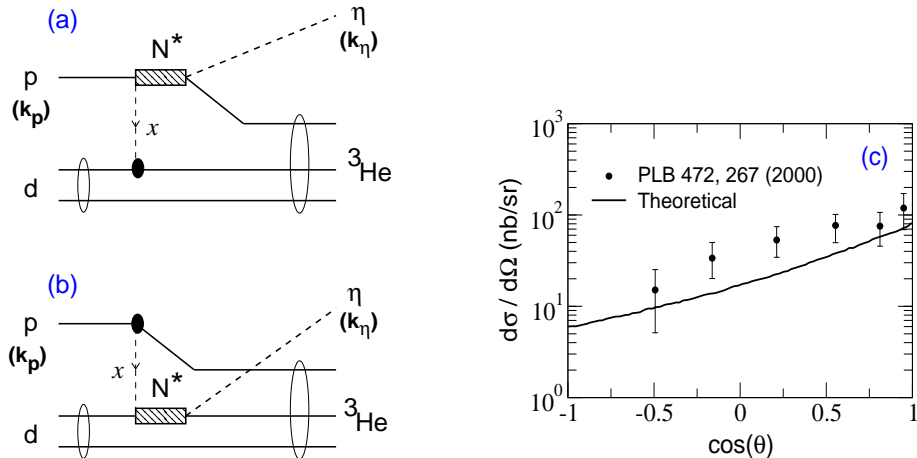


**Figure 10.** Schematic diagram for the  $pd \rightarrow {}^3\text{He} \eta$  reaction with (a) projectile excitation and (b) target excitation.  $x$  denotes the exchanged meson which can be  $\pi$ ,  $\eta$ ,  $\rho$  or  $\omega$  meson. In (c) is shown the angular distribution of the  $\eta$  meson at a beam energy of 88.5 MeV above threshold. The data are from Ref. [69] and the solid line from [57].

The total cross sections obtained by integrating Eq. (27) over all angles also reproduced the data up to 1 GeV beam energy very well. The sensitivity of cross sections to different exchanged mesons in the transition potential was also studied. The authors find that though the  $\rho$ -exchange contribution dominates, contributions due to exchange of  $\omega$  and  $\pi$  are also important. It may, however, be mentioned that above calculations do not include FSI between  $\eta$  and  ${}^3\text{He}$ , whose effect could be significant near threshold.

The above results [57] contradict the findings of some earlier works in literature. In [40] for example, the authors evaluate the transition amplitude corresponding to the diagram (2) in Figure 7. Though the diagram appears similar to that in Figure (10), the transition amplitude is evaluated in a very different way. Apart from some Clebsch-Gordon coefficients, it is written in terms of the transition matrix for the  $\pi^+ d \rightarrow pp$  reaction and an overlap of the deuteron and  ${}^3\text{He}$  wave functions. The authors in [40] compare their calculation with data on the  $pd \rightarrow {}^3\text{He} \eta$  reaction up to 2.5 GeV, however, only at one angle, namely,  $\theta_\eta = 180^\circ$ . They mention the three body mechanism to be the appropriate choice since the two body graphs (see Figure 7) underestimate the data by two orders of magnitude. Conclusions similar to those of Ref.[40] regarding the role of the one and two step mechanisms, however for the  $pd \rightarrow pd\eta$  reaction were obtained in [61]. Finally we mention the findings of Ref. [130] where the authors studied the reaction mechanisms for the  $pd \rightarrow {}^3\text{H}_\Lambda K^+$  reaction. We mention these results since

the  $K^+$  is almost as heavy as the  $\eta$  meson and hence the kinematics and the momentum transferred to the nucleus in this reaction must be similar to that in the  $pd \rightarrow {}^3\text{He} \eta$  reaction. The angular distributions of the  $K^+$  mesons using the two step model are also backward peaked at high energies as in case of the  $\eta$ 's. The one step model produces forward peaked angular distributions, however, reduces the cross sections by 2-3 orders of magnitude.

In summary we can say that the various calculations in literature point toward some missing components in the understanding of the reaction mechanisms of the  $pd \rightarrow {}^3\text{He} \eta$  reaction. All these works do seem to agree on one point that the forward peaked angular distributions cannot be reproduced within the two step model and that the one step model does reproduce the forward peaking. However, they do not agree on the magnitude of the cross sections produced within the one step model. Hence, it would be useful to perform further investigations of the  $pd \rightarrow {}^3\text{He} \eta$  reaction within the one boson exchange model using more refined wave functions and including the effects of the final state interaction. It would be useful to obtain more data on this reaction at high energies in future.

## 5. Eta meson interaction with nuclei in the final state

Though the main objective of the entire eta meson related program has been the study of the eta nucleus interaction and location of eta mesic states, the extraction of this information from available data is often based on approximate methods. In the subsequent sections we point out the importance of few body equations and their application to study the effects of the  $\eta$ -nucleus interaction in the final states of the  $pn \rightarrow d\eta$ ,  $pd \rightarrow pd\eta$  and the  $p{}^6\text{Li} \rightarrow {}^7\text{Be} \eta$  reactions.

### 5.1. Approximate methods and the need for few body equations

As is evident from Figure 8,  $\eta$ -producing reaction amplitudes show a strong energy dependence close to threshold but seem to approach a constant value for large excess energies. Theoretical analyses attribute the sharp rise to the final state interaction (FSI) between the  $\eta$  and the nucleus. The interaction is dominantly  $s$ -wave and its effect reduces rapidly away from threshold. The above features seem to make it a good candidate for the use of the Watson-Migdal approximation [90] which is indeed often used (with a further simplification) in the analysis of eta producing reactions. In what follows, we briefly explain this approximation and the related conclusions about eta-nucleus scattering lengths drawn from it. We then go over to the incorporation of the FSI using a few body transition matrix and point out the drawbacks of the use of an on-shell approximation (such as the one mentioned above) for the FSI.

*5.1.1. Scattering length approximation* Within the approach of Watson and Migdal, the energy dependence of the reaction is determined by the on-shell scattering amplitude

of the final state [91], namely,

$$f_{FSI}(k) = \frac{1}{k \cot \delta - ik}, \quad (29)$$

where  $k$  for example is the center of mass momentum of the  $\eta$  and the nucleus and  $\delta$  the corresponding  $s$ -wave phase shift which near threshold can be approximated by the effective range expansion

$$k \cot \delta = \frac{1}{a} + \frac{r_0}{2}k^2 + \dots, \quad (30)$$

where  $a$  is the scattering length. If we simplify the above expression further by neglecting terms of order  $k^2$  and higher, the squared reaction amplitude for an  $\eta$  producing reaction can be written as

$$|f|^2 = f_B \times \frac{|a|^2}{1 + 2k\Im m a + |a|^2 k^2} \quad (31)$$

where  $f_B$  represents the squared amplitude in the absence of FSI. As we move away from threshold, the  $k^2$  term in Eq. (30) will be negligible only if the effective range parameter  $r_0$  is much smaller than  $a$ . The form that is more often used in the context of the eta-nucleus FSI is

$$|f|^2 = |f_p|^2 \times \frac{1}{(1 + 2k\Im m a + |a|^2 k^2)} \quad (32)$$

where  $|f_p|^2$  is an arbitrary factor fitted to reproduce the correct magnitude of the cross sections.

In [131], the author reproduced the data on the squared amplitude  $|f|^2$  for the  $pd \rightarrow {}^3\text{He} \eta$  reaction using the above approximation along with an eta-nucleus scattering length,  $a_{\eta^3\text{He}} = -2.31 + i 2.57$  fm, which was obtained by using the lowest order optical potential for the  $\eta^3\text{He}$  system. With the potential given as,

$$2 m_{\eta N}^R V_{opt}(r) = -4\pi A \rho(r) a_{\eta N}, \quad (33)$$

the phase shift could also be determined. This enabled the author to use the better approximation in Eq. (29) rather than just the one in Eq. (32) and little difference between the two results was found. However, the normalization factor in both cases was simply a free parameter.

*5.1.2. Half-off-shell  $\eta$ -nucleus  $T$ -matrix* In a proper description of the FSI between the  $\eta$  and the nucleus, one must consider the fact that the  $\eta$  meson can also be produced off the mass shell and eventually brought on-shell due to its interaction with the nucleus. In a few body approach, the off-shellness enters the theory by expressing the final state wave function as a solution of the Lippmann-Schwinger equation, written as

$$\langle \Psi^-(\vec{k}) | = \langle \vec{k} | + \int \frac{d\vec{q}}{(2\pi)^3} \frac{\langle \vec{k} | T | \vec{q} \rangle}{E(k) - E(q) + i\epsilon} \langle \vec{q} |, \quad (34)$$

where  $k$  is the final state c.m. momentum. The half-off-shell  $\eta$ -A  $T$ -matrix,  $\langle \vec{k} | T | \vec{q} \rangle$  is generated by solving few-body equations for the  $\eta$ -A system. The propagator in the

scattering term generates two terms originating from the principal-value and the residue parts. Physically they represent the off-shell and the on-shell scattering between the particles in the final state. We shall see below that the contribution of the rescattering of off-shell particles in the final state is indeed large and the off-shell term contributes much more to the FSI than the on-shell rescattering term.

In Figure 11a, we compare the amplitude squared  $|f|^2$  generated using few body equations for the  $\eta^3\text{He}$  FSI [60] with data [34]. The elementary  $\eta N$  t-matrix which is chosen to be the input to the few body calculation leads to an  $\eta N$  scattering length of (0.88, 0.41) fm and the few body t-matrix produces  $a_{\eta^3\text{He}} = (2.41, 5.71)$  fm. One can see in Figure 11b that the scattering length approximation (SLA) of Eq. (32) with a value of  $a_{\eta^3\text{He}} = (-2.31, 2.57)$  fm as in [131] reproduces the data equally well too. If on the other hand, we choose to use the value of  $a_{\eta^3\text{He}} = (2.41, 5.71)$  fm as obtained from the few body equations with the same multiplicative factor of  $|f_p|^2 = 2$ , the SLA underestimates the data. The purpose of this exercise is to emphasize that any conclusions about the magnitude or sign of the eta-nucleus scattering length based on fits to data using the SLA with arbitrary multiplicative factors can be quite misleading.

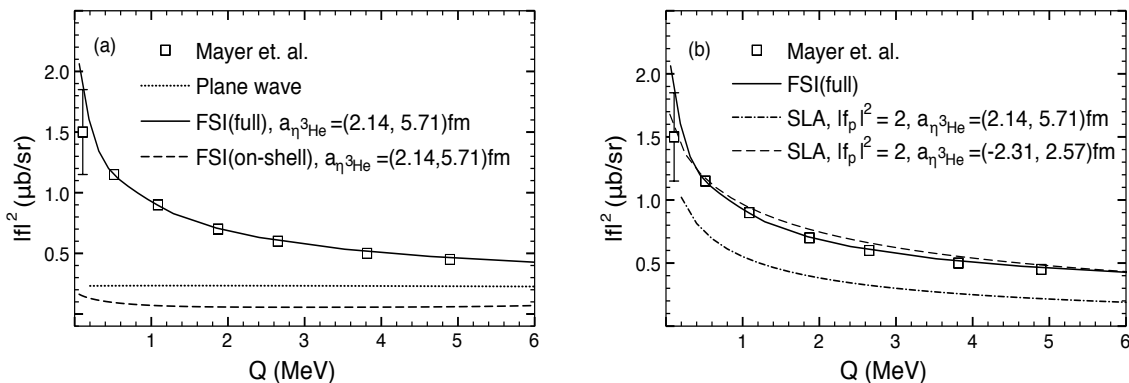


**Figure 11.** Importance of off-shell rescattering in the  $pd \rightarrow {}^3\text{He} \eta$  reaction with (a) showing the contribution of the on-shell term in the few body transition matrix [60] and (b) a comparison of the full few body calculation with the scattering length approximation using the  $\eta^3\text{He}$  scattering length obtained in [131] (dashed line) and the scattering length obtained from the few body t-matrix (dash-dotted line).

Recognizing the significance of the few body approach, we present in the next subsection a discussion of the  $pn \rightarrow d\eta$ ,  $pd \rightarrow pd\eta$  and the  $p{}^6\text{Li} \rightarrow \eta{}^7\text{Be}$  reactions where use of few body equations to describe the final state interaction between  $\eta$  mesons and nuclei is made.

## 5.2. Final state $\eta$ nucleus interaction in proton induced reactions

We begin the discussions in this section with the simplest eta-nucleus system, namely, the  $\eta$ -deuteron system and then go over to the  $\eta{}^7\text{Be}$  case. The  $pd \rightarrow \eta^3\text{He}$  reaction

which has been discussed in the earlier sections will not be dealt with over here. In what follows, we shall present three different approaches used to describe the  $\eta d$  interaction using few body equations.

*5.2.1. The  $pn \rightarrow d\eta$  reaction* The cross sections for the  $pn \rightarrow d\eta$  reaction were calculated in a series of works by Garcilazo and Peña [118, 132, 133] and various aspects of the production mechanism as well as the initial and final state interaction were studied. The production mechanism involved the exchange of the  $\pi$ ,  $\eta$ ,  $\sigma$  and heavier mesons as shown in Figure (12a). The final state  $\eta d$  interaction was described by using Faddeev equations for  $\eta d$  elastic scattering (see Figure (12b)). In [118], the authors used a non-relativistic three body model of the  $\eta NN$  system where all three particles interacted through pairwise interactions which were represented with separable potentials. The orbital states between the spectator particles and the center of mass of interacting pairs were restricted to s-waves. The relative orbital states for the interacting pairs were taken as  $S_{11}$  for the eta-nucleon pair and  ${}^3S_1$  for the nucleon-nucleon pair.

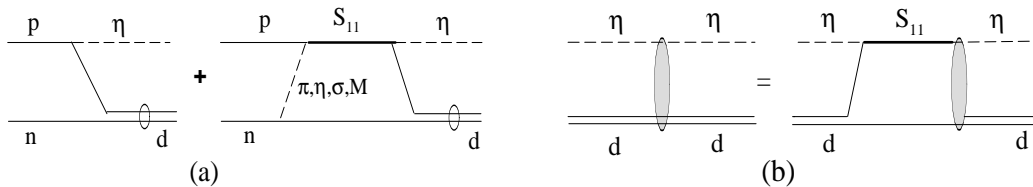


**Figure 12.** Model for (a) production mechanism and (b) final state interaction in the  $pn \rightarrow d\eta$  reaction.

The authors performed calculations using different inputs of the  $\eta N$  interaction corresponding to a range of  $\eta N$  scattering lengths. The overall agreement with data, including that at higher energies was found for a small value of the real part of the scattering length, namely 0.42 fm. The non-relativistic calculations in [118] were followed by a relativistic version [132] of the three body equations which incorporated relativistic kinematics and the boost of two-body meson-nucleon and nucleon-nucleon interactions. Though the boost effects were found to be small, relativistic effects on the range and strength of the pion exchange contribution to the reaction mechanism were found to be large. Apart from these results the authors also found that the initial state interaction, in general, is responsible for a reduction in the magnitudes of the cross sections. Continuing with the relativistic calculations, in [133] the authors considered the effects of taking into account the width of the  $\sigma$  meson in their model which involves the coupled  $\eta N$ - $\pi N$ - $\pi\pi N$  subsystems. The  $\pi\pi N$  channel is represented by an effective  $\sigma N$  channel and the authors performed calculations for the cases where (i) the  $\sigma$  and  $\pi$  masses are related by  $m_\sigma = 2m_\pi$  and no width is considered and (ii) the mass and the width of the  $\sigma$  meson are taken from  $\pi\pi$  scattering data. The results obtained in [118, 133] are shown in Figure 13.

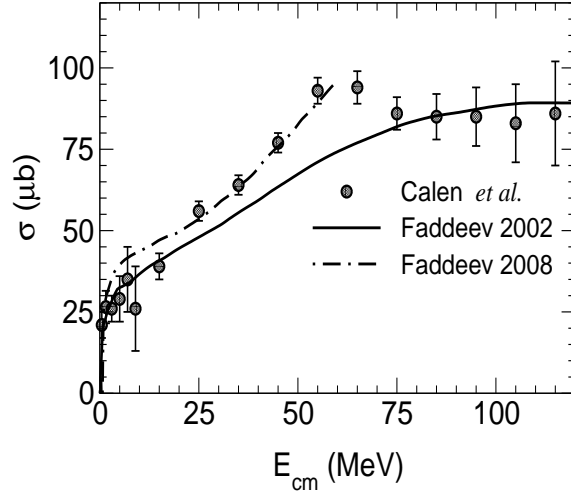


**Figure 13.** Cross sections for the reaction  $pn \rightarrow d\eta$  from a non-relativistic Faddeev calculation (solid line) [118] and a later calculation by the same authors using a relativistic approach (dash dotted line) [133]. The latter calculation takes into account the finite width of the  $\sigma$  meson and was performed at close to threshold energies. The data are from Ref. [89].

*5.2.2. The  $pd \rightarrow pd\eta$  reaction* A complete set of data covering the excess energy from around threshold to 107 MeV exist on the  $pd \rightarrow pd\eta$  reaction [39, 70, 71]. These data include the invariant mass distribution (integrated over other variables) for the  $\eta d$ ,  $\eta p$ , and  $pd$  systems. Out of them, like in the case of the  $pd \rightarrow {}^3\text{He} \eta$  reaction, the (inclusive)  $\eta d$  mass distribution exhibits a large enhancement near threshold, hence indicating a strong  $\eta d$  attraction. The  $pd \rightarrow pd\eta$  reaction, therefore, like the  $pd \rightarrow {}^3\text{He} \eta$  reaction has been studied theoretically in detail. However, due to the fact that there are three particles in the final state, the incorporation of the FSI is much more complicated in this reaction. One theoretical effort to understand these data is made in [123] where the authors essentially explore the role of different reaction mechanisms in the production amplitude, but do not include the FSI. In what follows we shall discuss Ref. [61] where a detailed study including the interaction amongst all the three particles is made.

The differential cross section for the  $pd \rightarrow pd\eta$  reaction, in the center-of-mass system, can be written as [61]

$$d\sigma = \frac{m_p^2 m_d^2}{2(2\pi)^5 s |\vec{k}_p|} d\Omega_{p'} |\vec{k}_{p'}| dM_{\eta d} |\vec{k}_{\eta d}| d\Omega_{\eta d} \frac{1}{6} \langle |T_{pd \rightarrow pd\eta}|^2 \rangle. \quad (35)$$

The  $T$ -matrix which includes the interaction between the  $\eta$  and the deuteron is given by,

$$\begin{aligned} T_{pd \rightarrow pd\eta} &= \langle \psi_{\eta d}(\vec{k}_{\eta d}), \vec{k}_{p'}; m_{p'}, m_{d'} | t_{pd \rightarrow pd\eta} | \vec{k}_p, \vec{k}_d; m_p, m_d \rangle \\ &= \langle \vec{k}_{\eta d}(\vec{k}_{\eta d}), \vec{k}_{p'}; m_{p'}, m_{d'} | t_{pd \rightarrow pd\eta} | \vec{k}_p, \vec{k}_d; m_p, m_d \rangle \\ &+ \sum_{m'_2} \int \frac{d\vec{q}}{(2\pi)^3} \frac{\langle \vec{k}_{\eta d}; m_{d'} | t_{\eta d} | \vec{q}; m'_2 \rangle}{E(k_{\eta d}) - E(q) + i\epsilon} \langle \vec{q}, \vec{k}_p; m'_2, m_{p'} | t_{pd \rightarrow pd\eta} | \vec{k}_p, \vec{k}_d \rangle; m_p, m_d \end{aligned} \quad (36)$$

where  $m_p$ ,  $m_d$ ,  $m_{p'}$ , and  $m_{d'}$  are the proton and the deuteron spin projections respectively. The second line in the above equation comes after replacing for  $\psi_{\eta d}(\vec{k}_{\eta d})$  using the Lippmann Schwinger equation. The  $\eta$  d FSI is contained in the  $\eta$  d elastic scattering t-matrix which is given as [41],

$$t_{\eta d}(\vec{k}', \vec{k}; z) = \langle \vec{k}'; \psi_0 | t^0(z) | \vec{k}; \psi_0 \rangle + \epsilon \int \frac{d\vec{k}''}{(2\pi)^3} \frac{\langle \vec{k}'; \psi_0 | t^0(z) | \vec{k}''; \psi_0 \rangle}{(z - \frac{k''}{2\mu})(z - \epsilon - \frac{k''}{2\mu})} \quad (37)$$

within the finite rank approximation (FRA). The FRA implies that the intermediate nucleus in the off shell scattering remains in the ground state.  $t^0(z)$  is an auxiliary t-matrix which is expressed in terms of the elementary  $\eta N$  t-matrix (see Ref. [41]).

Another prescription used in [61] involves a factorization of the half-off-shell  $\eta d$  t-matrix into an on-shell part expressed using the effective range expansion and off-shell form factors. Thus [61],

$$t_{\eta d}(\vec{k}', \vec{k}; z(k_0)) = g(k, k_0) \frac{F_{\eta d}(z(k_0))}{(2\pi)^2 \mu_{\eta d}} g(k', k_0), \quad (38)$$

with

$$F_{\eta d}(k) = \left( \frac{1}{a} + \frac{1}{2} r_0 k^2 + s k^4 - ik \right)^{-1}.$$

The off shell form factor is written in terms of the deuteron wave function as  $g(k', k_0) = \int d^3r j_0(rk'/2) \phi_d^2(r) j_0(rk_0/2)$ . The effective range parameters  $a$ ,  $r_0$  and  $s$  are taken from the relativistic Faddeev calculation in [26].

The  $pd$  FSI in [61] is included using the Watson-Migdal approach [90, 134], by multiplying the  $T$ -matrix in (36) with the Coulomb interaction modified inverse Jost function,  $[J(p)]^{-1}$ . The interaction between the  $\eta$ -meson and the proton in the final state, to a certain extent, is contained implicitly in the calculations because in the two-step reaction model the  $\pi^+ N \rightarrow \eta N$  vertex is described by a  $T$ -matrix. The production matrix for the  $pd \rightarrow pd\eta$  reaction in the two-step model is given by

$$\begin{aligned} < |T_{pd \rightarrow pd\eta}| > = \frac{3}{2} i \int \frac{d\vec{k}_\pi}{(2\pi)^3} \sum_{int m's} < pn | d > < \pi d | T_{pp \rightarrow \pi d} | pp > \\ & \times \frac{1}{(k_\pi^2 - m_\pi^2 + i\epsilon)} < \eta p | T_{\pi N \rightarrow \eta p} | \pi N > \end{aligned} \quad (39)$$

where  $\vec{k}_\pi$  is the momentum of the exchanged pion and details of the dependence of the integrand on it can be found in [61]. This  $T$ -matrix is evaluated using the Paris parametrization [124] for the deuteron wave function. The  $pd$  Jost function is included for both, the spin-doublet and spin-quadruplet states of the  $pd$  system. The expression and details of the Jost function are given in [61].

The full squared amplitude along with the data is shown in Figure 14 including only the  $\eta d$  FSI (shown by dot-dashed line) and the  $\eta d$  and  $pd$  FSI (shown by the solid line) as a function of the excess energy. The  $\eta d$  FSI is included within the factorized  $\eta$  d t-matrix approach. Two results emerge from here: (1) the enhancement of the observed squared production amplitude near threshold is fully described by the FSI and (2) while

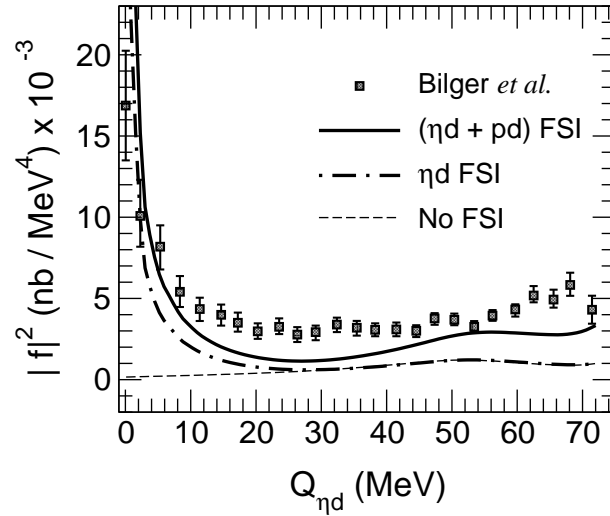


**Figure 14.** Effects of the  $\eta d$  and  $pd$  FSI on the squared amplitude of the  $pd \rightarrow pd\eta$  reaction at a beam energy of 1032 MeV. The  $\eta d$  FSI is given by the factorized prescription using the parameter set corresponding to  $a_{\eta N} = 1.07 + i0.26$  fm from Ref. [26].  $Q_{\eta d}(= M_{\eta d} - m_{\eta} - m_d)$  is the excess energy of the  $\eta d$  system with  $M_{\eta d}$  being the  $\eta d$  invariant mass. The data are from Ref. [39] and theoretical results from [61].

the effect of the  $\eta d$  FSI is limited to the excess energy near threshold, the  $pd$  FSI persists over the whole energy range.

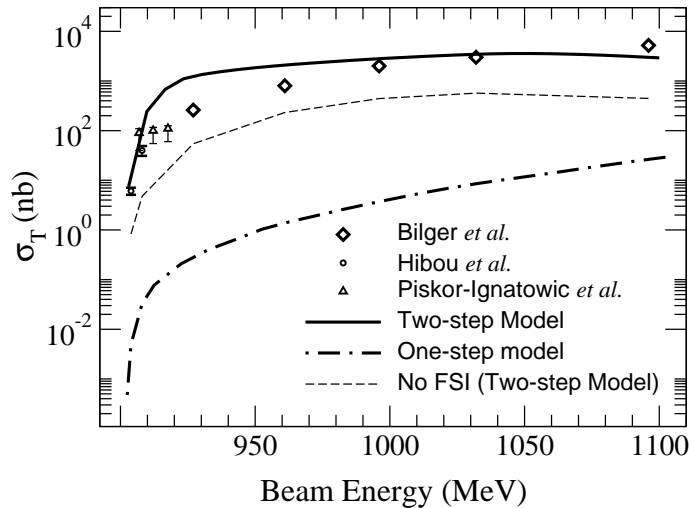


**Figure 15.** The total cross sections for the  $pd \rightarrow pd\eta$  reaction. The data from Ref. [39, 70, 71] are shown by rhombuses, circles and triangles respectively. Theoretical results are from [61].

The results for the total cross sections are shown in Figure 15, where the dashed line represents the plane wave results while the solid line corresponds to the calculated cross sections including both the  $\eta d$  and  $pd$  FSI. The  $\eta d$  FSI is evaluated using the factorized prescription for the parameter set corresponding to  $a_{\eta N} = 1.07 + i0.26$  fm taken from the relativistic Faddeev calculation of Ref. [26]. It can be seen that a general agreement



with the measured cross section is achieved after both the  $\eta d$  and  $pd$  FSI are included.

As discussed in Section 4.1, the contribution of the one-step model is found to be suppressed near the threshold of the meson producing reactions because of the large momentum transfer. For completeness, the total cross sections calculated using the one-step model for the  $pd \rightarrow pd\eta$  reaction are shown by the dot-dashed line in Figure 15. The details of this calculation can be found in [61].

*5.2.3. Cluster model approach to the  $p^6\text{Li} \rightarrow \eta^7\text{Be}$  reaction* As seen in the earlier sections, the measured cross sections near the threshold of eta production in  $pn$  and  $pd$  collisions show large enhancements, which are shown to arise from the strong final state interaction between the  $\eta$  meson and  $^3\text{He}$  or deuteron. This strong FSI is also shown to give rise to quasi-bound eta states in these nuclei. This observation naturally raises the curiosity if such a strong eta-nucleus FSI also exists in heavier nuclei, indicating thereby the possibility for the existence of quasi-bound states in them. The first measurement to explore this possibility was done in 1993 [72] by the Turin Group for the  $p^6\text{Li} \rightarrow \eta^7\text{Be}$  reaction at the beam energy of 683 MeV (excess energy of 19 MeV). The differential cross section was found to be  $4.6 \pm 3.8$  nb/sr around 20 degrees.

A theoretical analysis of this reaction was first performed in [63] within a cluster model. With the  $^6\text{Li}$  and  $^7\text{Be}$  nuclei considered to be  $d\text{-}\alpha$  and  $^3\text{He}\text{-}\alpha$  clusters, the  $^6\text{Li}(p, \eta)^7\text{Be}$  reaction proceeds via the intermediate  $d(p, \eta)^3\text{He}$  reaction. Performing a simple calculation where the cross section for the  $^6\text{Li}(p, \eta)^7\text{Be}$  reaction appears as

$$\left(\frac{d\sigma}{d\Omega}\right)_{^6\text{Li}(p,\eta)^7\text{Be}} = (\text{kinematic factors}) \times |F_L(Q)|^2 \left(\frac{d\sigma}{d\Omega}\right)_{d(p,\eta)^3\text{He}}, \quad (40)$$

the authors found a good agreement with data for a certain choice of the nuclear form factor  $F_L(Q)$ . The final state interaction (FSI) between the  $\eta$  meson and the nucleus was not included and the need for improving the simple estimate was mentioned.

A more detailed and complete theoretical study of the  $p^6\text{Li} \rightarrow \eta^7\text{Be}$  reaction has been done recently [64]. This work also uses the cluster model description of the target and the recoiling nuclei (see Figure 16(a)). Since the reaction is modelled to proceed via the  $pd[\alpha] \rightarrow ^3\text{He}[\alpha]\eta$  reaction with the  $\alpha$  remaining a spectator, the  $\eta$  production is governed by the  $T$ -matrix for the  $pd \rightarrow ^3\text{He}\eta$  reaction. Following the work presented in Section 4.2 this  $T$ -matrix is constructed microscopically using the two-step model. Neglecting the effect of Fermi motion on the  $pd \rightarrow ^3\text{He}\eta$  production amplitude, the  $T$ -matrix for the  $p^6\text{Li} \rightarrow \eta^7\text{Be}$  reaction is written as

$$\begin{aligned} \langle |T_{p^6\text{Li} \rightarrow \eta^7\text{Be}}| \rangle &= i^{(L+1)} \sqrt{4\pi} \sum_{M\mu} Y_{LM}^*(\hat{Q}) F_L(Q) \\ &\times \langle J, m_7' | 1/2, \mu, L, M \rangle \langle |T_{pd \rightarrow \eta^3\text{He}}| \rangle, \end{aligned} \quad (41)$$

where the transition form factor for  $^6\text{Li} \rightarrow ^7\text{Be}$ ,  $F_L(Q)$ , is expressed as

$$F_L(Q) = \int_0^\infty r^2 dr \Psi_l^{*7}(r) j_L(Qr) \Psi_0^6(r) \quad (42)$$

with the momentum transfer  $\vec{Q} = \frac{4}{7}\vec{k}_\eta - \frac{2}{3}\vec{k}_p$ .  $\Psi_0^6(r)$  and  $\Psi_l^{*7}(r)$  are the radial wave functions for the relative motion of the clusters in  ${}^6\text{Li}$  and  ${}^7\text{Be}$  respectively generated using a Wood-Saxon potential [135].

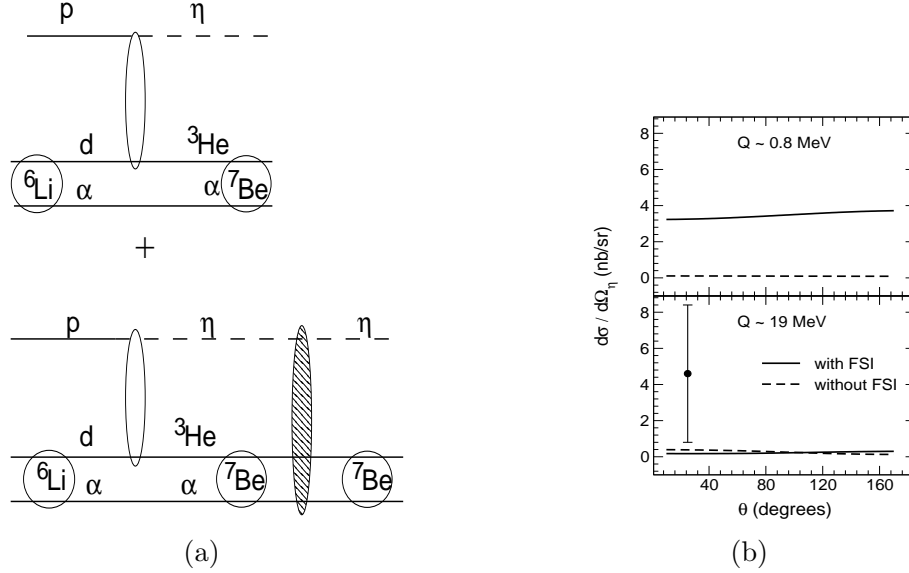


**Figure 16.** The  $p{}^6\text{Li} \rightarrow \eta{}^7\text{Be}$  reaction: (a) Schematics of the cluster model approach. (b) Angular distributions for different excess energies,  $Q$ . The data point is by the Turin group [72]. The calculations [64] are shown for the ground state of the  ${}^7\text{Be}$  nucleus.

The FSI between the  $\eta$  meson and  ${}^7\text{Be}$  is taken into account as discussed before by writing the wave function  $\psi_{\eta{}^7\text{Be}}$  in the final state using the Lippmann Schwinger equation with an elastic  $\eta$ - ${}^7\text{Be}$  transition matrix. The latter is evaluated assuming the  $\eta$ - ${}^7\text{Be}$  interaction to be a three body  $\eta$ - ${}^3\text{He}$ - ${}^4\text{He}$  problem. Thus the  $\eta$ - ${}^7\text{Be}$  t-matrix is written as,

$$T_{\eta{}^7\text{Be}}(\vec{k}', \vec{k}, z) = \int d^3x |\Psi_L^7(x)|^2 (T_1(\vec{k}', \vec{k}, a_1\vec{x}, z) + T_2(\vec{k}', \vec{k}, a_2\vec{x}, z)), \quad (43)$$

where  $T_1$  and  $T_2$  are the medium modified t-matrices for the off-shell  $\eta$  scattering on the bound  ${}^3\text{He}$  and  ${}^4\text{He}$ .  $\vec{x}$  is the relative coordinate between  ${}^3\text{He}$  and  ${}^4\text{He}$  and  $\vec{r}_1 = a_1\vec{x}$  and  $\vec{r}_2 = a_2\vec{x}$  are the coordinates of the 2 nuclei with respect to the mass-7 center of mass system (with  $a_1 = 4/7$  and  $a_2 = -3/7$ ).  $\Psi_L^7$  represents the inter cluster wave function with angular momentum  $L$ .  $T_1$  and  $T_2$  are themselves written using a Faddeev type decomposition. As a result, the  $\eta$  meson produced in the final state can undergo multiple off-shell scatterings on the  ${}^3\text{He}$  and  ${}^4\text{He}$  nuclei until it finally emerges as an on-shell meson.

Figure 16 shows the angular distributions of the eta meson for different excess energies along with the reaction diagram. The angular distributions are seen to remain isotropic at all energies considered and the FSI is found to enhance the cross sections near threshold.

Figure 17 shows the total cross sections as a function of the beam energy summed over all possible low lying bound states of the  ${}^7\text{Be}$  nucleus ( $L = 1, 3$  included) as well as

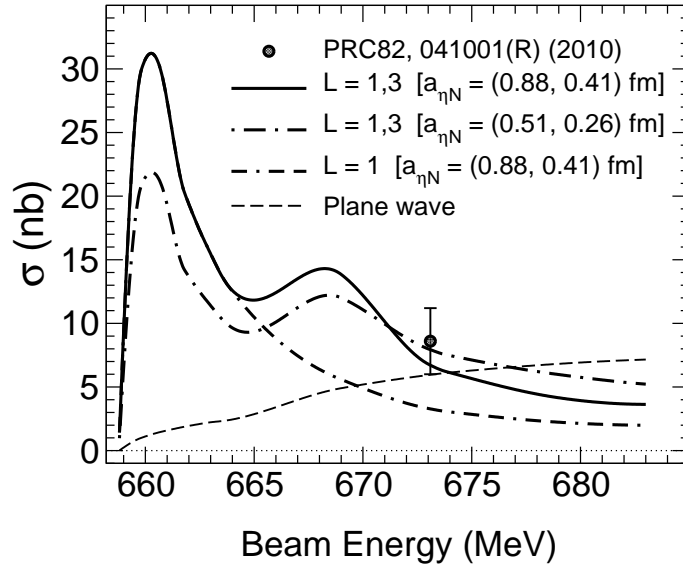


**Figure 17.** Total cross sections for the  $p^6\text{Li} \rightarrow \eta^7\text{Be}$  reaction. The solid, dash-dotted and dot-double dashed lines are obtained with calculations [64] including the  $\eta^7\text{Be}$  FSI. The data point was measured for the ground state of  $^7\text{Be}$ .

for the case where  $L = 1$ . The solid and the dot-dashed lines in the figure correspond to the results including  $\eta^7\text{Be}$  FSI for two different inputs of the  $\eta N$  interaction with scattering lengths,  $a_{\eta N} = (0.88, 0.41)$  fm [127] and  $(0.51, 0.26)$  fm [12]. The result with only  $L = 1$  contribution is shown by the double dash-dotted line. The figure also shows the results without FSI between  $\eta$  and  $^7\text{Be}$ , represented by the dashed lines. As in case of  $A=2-4$  nuclei, here also the FSI leads to a large enhancement in the cross sections up to about 15 MeV excess energy. Two bumps are seen in the inclusive distribution. They arise due to different binding energies of the different states of  $^7\text{Be}$ , leading to different threshold energy for them (for details see Ref. [64]). The data point is from a recent measurement of the total cross section made by the COSY collaboration [75] for the ground state of  $^7\text{Be}$ .

This work also determines the scattering length for the  $\eta^7\text{Be}$   $T$ -matrix describing the FSI in the calculations for several values of the  $\eta N$  scattering length which enter as an input in the calculations. This is done to explore the possible existence of any  $\eta^7\text{Be}$  mesic state. There seems some indication for such states for large values of  $a_{\eta N}$ , however it would indeed be premature to conclude anything about it. It may be better to perform a time delay analysis or a  $K$ -matrix analysis for the above  $\eta^7\text{Be}$   $T$ -matrix.

## 6. Summary

The  $\eta$  meson due to its strong attractive interaction with a nucleon has turned out to be the most promising candidate for the exploration of exotic states of mesons and nuclei. A survey of the theoretical and experimental efforts which triggered and kept the search for  $\eta$ -mesic nuclei alive for the past twenty five years has been performed in

the present work. In what follows, we summarize some global and specific observations which emerge from this survey.

- (i) A good estimate of the strength of the  $\eta$ -nucleon ( $\eta N$ ) interaction is crucial for the interpretation of the data on  $\eta$  meson production on nuclei and the theoretical prediction of  $\eta$ -mesic nuclei. With the possibility of obtaining  $\eta$ -nucleon elastic scattering data being ruled out due to the nonavailability of  $\eta$  beams, the  $\eta N$  interaction strength is quantified in terms of a scattering length,  $a_{\eta N}$ , determined from analyses of  $\eta$  production in pion, photon and proton induced reactions. Phenomenological and theoretical studies incorporating meson-baryon coupled channels and the relevant intermediate baryon resonances obtain a wide range of scattering lengths with  $0.18 \leq \Re a_{\eta N} \leq 1.03$  fm and  $0.16 \leq \Im a_{\eta N} \leq 0.49$  fm. Such a large spread exists despite the fact that the calculations have been done in the best possible way using different models.

A closer look at the various values of  $a_{\eta N}$  obtained in literature, however, demonstrates a curious fact. Most of the theoretical calculations find small values of the real part of  $a_{\eta N}$ . Though the phenomenological determinations in general find both small and big values, one of the most elaborate calculation involving nine baryon resonances and the  $\pi N$ ,  $\eta N$ ,  $\pi \Delta$ ,  $\rho N$  and  $\sigma N$  coupled channels finds  $a_{\eta N} = 0.3 + i 0.18$  fm which is very close to the very first prediction [1] of  $a_{\eta N} = 0.28 + i 0.19$  fm. A smaller  $\eta N$  scattering length would favour light  $\eta$  mesic nuclei [40] and heavy  $\eta$  mesic nuclei with lower binding energies [3,19].

- (ii) The experimental searches for the existence of  $\eta$  mesic nuclei can be broadly divided into two categories; one searching for a direct signal such as a peak in the missing mass spectra and the other hinting toward the existence of these states through a large enhancement of the  $\eta$  production cross sections near threshold. Whereas the former data, due to the difficulty in performing such experiments are scarce and not conclusive, the latter depends on theoretical models for interpretation. The theoretical model itself depends on two inputs, namely, the reaction mechanism used and the treatment of the final state interaction (FSI) between the  $\eta$  meson and nuclei. Many of the  $\eta$  production cross sections are reproduced well with values of  $a_{\eta N}$  much larger than those mentioned at the end of (i) above. To reach a definite conclusion one would have to be sure that both the treatment of FSI as well as the reaction mechanism involved bear little uncertainties. The FSI between the  $\eta$  mesons and nuclei is well determined if one uses few body equations rather than resorting to approximate methods for incorporating the FSI. The uncertainty in the FSI then could arise only from the possible inaccuracy of the  $\eta N$  transition matrix.

The reaction mechanism at threshold seems to be well understood within models based on the two step process. However, in Chapter 4 we saw that at energies away from threshold where the isotropic angular distributions of  $\eta$  mesons become forward peaked, limitations do exist in the understanding of the reaction

mechanisms. It could be that at higher energies, there exists an interference rather than just a single mechanism which explains the entire set of data. Further investigations filling up the missing elements in the already existing extensive works is timely.

- (iii) The few body treatment of the FSI shows that the large enhancement in the eta-production amplitude near threshold arises mainly due to off-shell scattering of the eta-meson in the final state. This means that at the production vertex, the  $\eta$  meson could in principle be produced off-shell, undergo multiple elastic scatterings from the nucleus and then get converted to an on-shell  $\eta$  due to its interaction with the nucleus. It is important to realize this aspect because many of the eta-meson production works in literature consider only the on-shell scattering of the eta meson in the FSI. Such calculations may necessitate using larger values for  $a_{\eta N}$  to reproduce the data and consequently may lead to unreliability in the conclusion about the possible existence of eta-nucleus bound states.
- (iv) The direct signal searches mentioned in (ii) were carried out using protons, pions and photons incident on various light nuclei. Some experiments did see the signals indicating the existence of an  $\eta$  mesic state but the results were not reconfirmed. The expectations from the future lie in the experiments planned at the J-PARC, MAMI and COSY facilities. The K1.8BR beamline at J-PARC for example will be used to perform the recoilless production and spectroscopy of  $\eta$  mesic nuclei using the  $(\pi^-, n)$  reaction and targets such as  ${}^7\text{Li}$  and  ${}^{12}\text{C}$  [136]. In Tables 1 and 2 of the present review we have collected the pole values of all possible unstable states of  $\eta$  mesons and nuclei. There exists the prediction for quasibound eta-mesic  ${}^6\text{He}$  states from a QCD based quark-meson coupling approach [23]. Quasibound states of  ${}^{12}\text{C}$  and  ${}^{16}\text{O}$  are predicted using different approaches [20, 21, 22, 23]. However, the pole values from the different approaches differ a lot. The predicted range of values can be taken as a guide for the experimental searches and the experimental finding of some eta-mesic states could in turn confirm the validity of one or more of the theoretical approaches used.

## References

- [1] Bhalerao R S and Liu L C 1985 *Phys. Rev. Lett.* **54** 865
- [2] Haider Q and Liu L C 1986 *Phys. Lett. B* **172** 257
- [3] Liu L C and Haider Q 1986 *Phys. Rev. C* **34** 1845
- [4] Cheng W K, Kuo T T S and Li G L 1987 *Phys. Lett. B* **195** 515
- [5] Chrien R E *et al* 1988 *Phys. Rev. Lett.* **60** 2595
- [6] Agnello M *et al* 2005 *Phys. Rev. Lett.* **94** 212303
- [7] Pandejee G M, Upadhyay N J and Jain B K 2010 *Phys. Rev. C* **82** 034608
- [8] Geissel H *et al* 2002 *Phys. Rev. Lett.* **88** 122301; 2002 *Phys. Lett. B* **549** 64; Yamazaki T, Hirenzaki S, Hayano R S and Toki H, 2012 *Phys. Rep.* **514** 1
- [9] Bhalerao R S 1987 *Phys. Rev. C* **35** 1592
- [10] Hosaka A 1992 *Phys. Lett. B* **293** 23; Gobbi C, Hosaka A and Scoccola N 1993 *Nucl. Phys. A* **562** 461

- [11] Green A M and Wycech S 1999 *Phys. Rev. C* **60** 035208
- [12] Green A M and Wycech S 2005 *Phys. Rev. C* **71** 014001; Green A M and Wycech S 2005 *Phys. Rev. C* **72** 029902(E)
- [13] Shyam R and Scholten O 2008 *Phys. Rev. C* **78** 065201
- [14] Durand J, Juliá-Díaz B, Lee T -S H, Saghai B and Sato T 2008 *Phys. Rev. C* **78** 025204
- [15] Inoue T, Oset E and Vicente Vacas M J 2002 *Phys. Rev. C* **65** 035204
- [16] Abdel-Bary, M *et al* 2003 *Phys. Rev. C* **68** 021603(R)
- [17] Coon S A and Scadron M D 1982 *Phys. Rev. C* **26** 562
- [18] Wilkin C 1994 *Phys. Lett. B* **331** 276
- [19] Magiera A and Machner H 2000 *Nucl. Phys. A* **674** 515
- [20] Haider Q and Liu L C 2002 *Phys. Rev. C* **66** 045208
- [21] Chiang H C, Oset E and Liu L C 1991 *Phys. Rev. C* **44** 738
- [22] García-Recio C, Inoue T, Nieves J and Oset E 2002 *Phys. Lett. B* **550** 47
- [23] Tsushima K, Lu D H, Thomas A W, Saito K 1998 *Phys. Lett. B* **443** 26
- [24] Bass S and Thomas A W 2006 *Phys. Lett. B* **634** 368
- [25] Ueda T 1991 *Phys. Rev. Lett.* **66** 297
- [26] Garcilazo H 2005 *Phys. Rev. C* **71** 048201
- [27] Garcilazo H and Peña M T 2001 *Phys. Rev. C* **63** 021001
- [28] Garcilazo H and Peña M T 2000 *Phys. Rev. C* **61** 064010
- [29] Wycech S and Green A M 2001 *Phys. Rev. C* **64** 045206
- [30] Wycech S, Green A M and Niskanen J A 1995 *Phys. Rev. C* **52** 544
- [31] Rakityansky S A, Sofianos S A, Sandhas W and Belyaev V B 1995 *Phys. Lett. B* **359** 33
- [32] Rakityansky S A, Sofianos S A, Braun M, Belyaev V B and Sandhas W 1996 *Phys. Rev. C* **53** 2043
- [33] Rakityansky S A, Belyaev V B, Sofianos S A, Braun M and Sandhas W 1996 *Chin. J. Phys.* **34** 998
- [34] Mayer B, Boudard A, Fabbro B, Garcon M, Kerboul C, Poitou J, Wellers F and Jacobs W W *et al* 1996 *Phys. Rev. C* **53** 2068
- [35] Berger J, Boivin M, Boudard A, Fleury P, Germond J F, Goldzahl L, Kerboul C and Mayer B *et al* 1988 *Phys. Rev. Lett.* **61** 919
- [36] Wronska A *et al* 2005 *Eur. Phys. J. A* **26** 421
- [37] Mersmann T, Khoukaz A, Buscher A, Chiladze D, Dymov S, Hartmann M, Hejny V and Kacharava A *et al* 2007 *Phys. Rev. Lett.* **98** 242301
- [38] Rausmann T *et al* 2009 *Phys. Rev. C* **80** 017001
- [39] Bilger R *et al* 2004 *Phys. Rev. C* **69** 014003
- [40] Laget J M and Lecolley J F 1988 *Phys. Rev. Lett.* **61** 2069
- [41] Kelkar N G, Khemchandani K P and Jain B K 2006 *J. Phys. G* **32** 1157; Kelkar N G, Khemchandani K P and Jain B K 2006 *J. Phys. G* **32** L19
- [42] Kelkar N G, Nowakowski M, Khemchandani K P and Jain S R 2004 *Nucl. Phys. A* **730** 121
- [43] Kelkar N G, Nowakowski M, and Khemchandani K P 2003 *Nucl. Phys. A* **724** 357
- [44] Kelkar N G 2007 *Phys. Rev. Lett.* **99** 210403
- [45] Pfeiffer M *et al* 2004 *Phys. Rev. Lett.* **92** 252001
- [46] Budzanowski A *et al* [COSY-GEM Collaboration] 2009 *Phys. Rev. C* **79** 012201
- [47] Betigeri M G *et al* [COSY-GEM Collaboration] 2007 *Nucl. Instrum. Meth. A* **578** 198
- [48] Laget J M, Wellers F and Lecolley J F 1991 *Phys. Lett. B* **257** 254
- [49] J F Germond and Wilkin C 1990 *Nucl. Phys. A* **518** 308
- [50] Santra A B and Jain B K 1998 *Nucl. Phys. A* **634** 309
- [51] Czyżykiewicz R *et al* 2007 *Phys. Rev. Lett.* **98** 122003
- [52] Shyam R 2007 *Phys. Rev. C* **75** 055201
- [53] Faeldt G and Wilkin C 1996 *Nucl. Phys. A* **604** 441
- [54] Faeldt G and Wilkin C 1995 *Nucl. Phys. A* **587** 769

- [55] Faeldt G and Wilkin C 1996 *Nucl. Phys. A* **596** 488
- [56] L A Kondratyuk and Yu N Uzikov 1997 *Phys. Atom. Nucl* **60** 468
- [57] Santra A B and Jain B K 2001 *Phys. Rev. C* **64** 025201
- [58] Khemchandani K P, Kelkar N G and Jain B K 2003 *Phys. Rev. C* **68** 064610
- [59] Khemchandani K P, Kelkar N G and Jain B K 2007 *Phys. Rev. C* **76** 069801
- [60] Khemchandani K P, Kelkar N G and Jain B K 2002 *Nucl. Phys. A* **708** 312
- [61] Upadhyay N J, Khemchandani K P, Jain B K and Kelkar N G 2007 *Phys. Rev. C* **75** 054002
- [62] Upadhyay N J, Khemchandani K P, Jain B K and Kelkar N G 2009 *Mod. Phys. Lett. A* **24** 2319
- [63] Al-Khalili J S, Wilkin C and Barbaro M B 1993 *J. Phys. G* **19** 403
- [64] Upadhyay N J, Kelkar N G and Jain B K 2009 *Nucl. Phys. A* **824** 70
- [65] Berthet P *et al* 1985 *Nucl. Phys. A* **443** 589
- [66] Smyrski J, Adam H -H, Budzanowski A, Czerwinski E, Czyzykiewicz R, Gil D, Grzonka D and Janusz M *et al* 2007 *Phys. Lett. B* **649** 258
- [67] Adam H -H, Geck I, Khoukaz A, Lister T, Santo R, Steltenkamp S, Taschner A and Czerwinski E *et al* 2007 *Phys. Rev. C* **75** 014004
- [68] Bilger R, Brodowski W, Calen H, Clement H, Ekstrom C, Faldt G, Fransson K and Gustafsson L *et al* 2002 *Phys. Rev. C* **65** 044608
- [69] Betigeri M *et al* [GEM Collaboration] 2000 *Phys. Lett. B* **472** 267
- [70] Hibou F *et al* 2000 *Eur. Phys. J. A* **7** 537
- [71] Piskor-Ignatowicz C, Smyrski J, Moskal P, Adam H -H, Budzanowski A, Czerwinski E, Czyzykiewicz R and Gil D *et al* 2007 *Int. J. Mod. Phys. A* **22** 528
- [72] Scomparin E *et al* 1993 *J. Phys. G* **19** L51
- [73] Ulicny M *et al* [GEM Collaboration] 2001 *AIP Conf. Proc.* **603** 543
- [74] Machner H *et al* 2006 *Acta Phys. Slov.* **56** 227
- [75] Budzanowski A *et al* [COSY-GEM Collaboration] 2010 *Phys. Rev. C* **82** 041001
- [76] Clajus M and Nefkens B M K 1992 *PiN Newslett.* **7** 76
- [77] Arndt R A, Briscoe W J, Strakovsky I I, Workman R L and Pavan M M 2004 *Phys. Rev. C* **69** 035213
- [78] Prakhov S *et al* 2005 *Phys. Rev. C* **72** 015203
- [79] Arndt R A, Briscoe W J, Morrison T W, Strakovsky I I, Workman R L and Gridnev A B 2005 *Phys. Rev. C* **72** 045202
- [80] Sauer mann Ch, Friman B L and Nörenberg W 1995 *Phys. Lett. B* **341** 261
- [81] Kaiser N, Waas T and Weise W 1997 *Nucl. Phys. A* **612** 297
- [82] Liu Y -R and Zhu S -L 2007 *Phys. Rev. D* **75** 034003
- [83] Sibirtsev A, Schneider S, Elster Ch, Haidenbauer J, Krewald S and Speth J 2002 *Phys. Rev. C* **65** 044007
- [84] Penner G and Mosel U 2002 *Phys. Rev. C* **66** 055211
- [85] Lutz M F M, Wolf Gy and Friman B 2006 *Nucl. Phys. A* **765** 495
- [86] Gasparyan A M, Haidenbauer J, Hanhart C and Speth J 2003 *Phys. Rev. C* **68** 045207
- [87] Johnson J D, Bureson G R, Edwards C, El-Ghossain M, Espy M A, Garnett R, Hussein A and Johnson K *et al* 1993 *Phys. Rev. C* **47** 2571
- [88] Haider Q and Liu L C 1987 *Phys. Rev. C* **36** 1636
- [89] Calen H, Dyring J, Fransson K, Gustafsson L, Haggstrom S, Hoistad B, Johanson J and Johansson A *et al* 1998 *Phys. Rev. Lett.* **80** 2069
- [90] M Goldberger and K M Watson 1964 *Collision Theory* (New York: Wiley)
- [91] Sibirtsev A, Haidenbauer J, Hanhart C and Niskanen J A 2004 *Eur. Phys. J. A* **22** 495
- [92] Frascaria R, Roudot F, Duval M A, Wurzinger R, Spang W, Ernst J, Hinterberger F and Jahn R *et al* 1994 *Phys. Rev. C* **50** 537
- [93] Budzanowski A *et al* [GEM Collaboration] 2009 *Nucl. Phys. A* **821** 193
- [94] Moskal P and Smyrski J 2010 *Acta Phys. Polon. B* **41** 2281
- [95] Hanhart C 2005 *Phys. Rev. Lett.* **94** 049101

- [96] Pfeiffer M, Thoma U, van Pee H, Ahrens J, Annand J R M, Beck R, Caselotti G and Cherepnaya S *et al* 2005 *Phys. Rev. Lett.* **94** 049102
- [97] Pheron F, Ahrens J, Annand J R M, Arends H J, Bantawa K, Bartolome P A, Beck R and Bekrenev V *et al* 2012 *Phys. Lett. B* **709** 21
- [98] Fujioka H 2010 *Acta Phys. Polon. B* **41** 2261
- [99] Sokol G A and Pavlyuchenko L N 2008 *Phys. Atom. Nucl.* **71** 509
- [100] Jaegle I [CBELSA-TAPS Collaboration] 2009 *Chin. Phys. C* **33** 1340; Krusche B [CBELSA/TAPS Collaboration] 2012 *AIP Conf. Proc.* **1441** 299
- [101] Moskal P 2011 *Fizika B* **20** 221
- [102] Nagahiro H, Jido D and Hirenzaki S 2009 *Phys. Rev. C* **80** 025205; Nagahiro H, Jido D and Hirenzaki S 2008 *Mod Phys Lett A* **23** 2512; Hirenzaki S, Nagahiro H and Jido D 2010 *AIP Conf. Proc.* **1322** 28
- [103] Ueda T 1984 *Phys. Lett. B* **141** 157
- [104] Shevchenko N V, Rakityansky S A, Sofianos S A, Belyaev V B and Sandhas W 1998 *Phys. Rev. C* **58** R3055
- [105] Green A M, Niskanen J A and Wycech S 1996 *Phys. Rev. C* **54** 1970
- [106] Shevchenko N V, Belyaev V B, Rakityansky S A, Sofianos S A and Sandhas W 2000 *Eur. Phys. J. A* **9** 143
- [107] Deloff A 2000 *Phys. Rev. C* **61** 024004
- [108] Haider Q and Liu L -C 2010 *J. Phys. G* **37** 125104
- [109] Inoue T and Oset E 2002 *Nucl. Phys. A* **710** 354
- [110] Jido D, Kolomeitsev E E, Nagahiro H and Hirenzaki S 2008 *Nucl. Phys. A* **811** 158
- [111] Nagahiro H, Jido D and Hirenzaki S 2005 *Nucl. Phys. A* **755** 491; Nagahiro H, Jido D and Hirenzaki S 2004 *Prog. Theor. Phys. Suppl.* **153** 340
- [112] Wigner E P 1955 *Phys. Rev.* **98** 145
- [113] Eisenbud L E 1948 *Ph.D. Thesis* Princeton University, unpublished
- [114] Smith F T 1960 *Phys. Rev.* **118** 349
- [115] Laget J M and Lecolley J F 1987 *Phys. Lett. B* **194** 177
- [116] Kondratyuk L A and Uzikov Yu N 1996 *Acta Phys. Polon. B* **27** 2977
- [117] Schonning K *et al* [CELSIUS/WASA Collaboration] 2009 *Phys. Rev. C* **79** 044002
- [118] Garcilazo H and Peña M T 2002 *Phys. Rev. C* **66** 034606
- [119] Nakayama K, Speth J and Lee T S H 2002 *Phys. Rev. C* **65** 045210
- [120] Nakayama K, Haidenbauer J, Hanhart C and Speth J 2003 *Phys. Rev. C* **68** 045201
- [121] Deloff A 2004 *Phys. Rev. C* **69** 035206
- [122] Grishina V Y, Kondratyuk L A, Buescher M, Hanhart C, Haidenbauer J and Speth J 2000 *Phys. Lett. B* **475** 9
- [123] Tengblad U, Faldt G and Wilkin C 2005 *Eur. Phys. J. A* **25** 267
- [124] Lacombe M, Loiseau B, Vinh Mau R, Cote J, Pires P and Turreil R de 1981 *Phys. Lett. B* **101** 139
- [125] Germond J F and Wilkin C 1988 *J. Phys. G* **14** 181
- [126] Arndt R A, Strakovsky I I, Workman R L and Bugg D V 1993 *Phys. Rev. C* **48** 1926
- [127] Fix A and Arenhovel H 2000 *Eur. Phys. J. A* **9** 119
- [128] Green A M and Wycech S 1997 *Phys. Rev. C* **55** R2167
- [129] Jain B K and Santra A B 1993 *Physics Report* **230** 1
- [130] Komarov V I, Lado A V and Uzikov Yu N 1995 *J. Phys. G* **21** L69
- [131] Wilkin C 1993 *Phys. Rev. C* **47** 938
- [132] Garcilazo H and Peña M T 2005 *Phys. Rev. C* **72** 014003
- [133] Garcilazo H and Peña M T 2008 *Eur. Phys. J. A* **38** 209
- [134] Gillespie J 1964 *Final State Interactions* (San Francisco: Holden-Day)
- [135] Buck B and Merchant A C 1988 *J. Phys. G* **14** L211; Kukulin V I, Neudatchin V G and Smirnov Y F 1975 *Nucl. Phys. A* **245** 429



- [136] Itahashi K, Fujioka H, Hirezaki S, Jido D and Nagahiro H *Spectroscopy of  $\eta$  mesic nuclei by  $(\pi^-, n)$  reaction at recoilless kinematics* Letter of Intent, [http://j-parc.jp/researcher/Hadron/en/pac\\_0707/pdf/LoI-itahashi.pdf](http://j-parc.jp/researcher/Hadron/en/pac_0707/pdf/LoI-itahashi.pdf)